EVALUATION OF COATED TOP FOIL BEARINGS: DRAG FRICTION COEFFICIENT, OPERATING DRAG TORQUE AND LIFT-OFF SPEED, AND DYNAMIC FORCE COEFFICIENTS

A Thesis

by

WONBAE JUNG

Submitted to the Office of Graduate and Professional Studies of
Texas A&M University
in partial fulfillment of the requirements for the degree of

MASTER OF SCIENCE

Chair of Committee,	Luis San Andrés
Committee Members,	Adolfo Delgado
	Stefan Hurlebaus
Head of Department,	Andreas Polycarpou

December 2017

Major Subject: Mechanical Engineering

ABSTRACT

Despite their many advantages, bump-type foil bearings (BFBs) have issues of dry-friction during sliding contact at rotor start/stop cycles. To prevent premature wear of both shaft and the BFB, the proper selection and application of a coating on the top foil is of importance to ensure bearing long life. This thesis presents measurements characterizing the static and dynamic load performance of a Generation I BFB having uncoated and coated (VN, TiSiN, MoS_2) top foils. The bearing, with length L and diameter D=38 mm, integrates a 360° 0.127 mm thick top foil made of Inconel X-750, and a 27 bumps strip layer, 0.47 mm in height, made of the same stock as for the top foils. The VN and TiSiN coating, 0.005 mm thick, applies to the front and back surfaces of a top foil. The MoS_2 coating, 0.020 mm thick, is sacrificial. The tests were conducted at room temperature (21°C).

The dry-sliding torque (T), recorded with a precision meter, increases linearly with an increase in applied static load (max $W/(LD)$=25.6 kPa). The bearing with a VN coated top foil shows the largest turning torque. The dry-sliding friction factor $f = T/(1/2\ WD)$ decreases as the specific load ($W/(LD)$) increases. As expected, journal rotation towards the top foil free end (clockwise) produces a larger f than for rotations in reverse.

A test-rig records the BFB drag torque during rotor acceleration and deceleration procedures to/from 70 krpm (138 m/s). The vertical load applied into a bearing equals $W/(LD)$= -8.0 kPa, 0 kPa and 8.0 kPa. In general, the bearing with a coated top foil shows a lesser drag torque than that of the uncoated top foil bearing. Among the coated foil

bearings, the bearing with VN coating shows the highest drag torque, whereas the one with MoS_2 shows the lowest. The drag torque increases with an increase in applied static load. Generally, the drag torque while the rotor is airborne is small (less than ~10% of peak torque). When the rotor starts up, the dry-sliding friction coefficient (f) of the bearing with VN coating is ~0.4 while f for the bearing with TiSiN coating is 0.3~0.4. The uncoated bearing shows the largest f ~0.6, and the MoS_2 coated one has the lowest f = 0.2~0.3.

Dynamic load tests spanning excitation frequencies (ω) from 200 Hz to 400 Hz serve to identify force coefficients for the test BFBs with a specific load of 16 kPa and operating with shaft speed at 50 krpm (833 Hz). Baseline measurements correspond to a null applied load and no shaft rotation. The test bearings show a remarkable behavior with nearly isotropic direct coefficients and very small cross-coupled ones. The bearing direct stiffnesses (K) increases with frequency, whereas the direct damping coefficients (C) quickly decrease. The bearing material loss factor, $\gamma=\omega C/K$, represents best the BFB ability to dissipate mechanical energy. Over the excitation frequency range, γ= 0.34, 0.28, and 0.12 for the uncoated, VN coated and TiSiN coated bearing. The test data show the bearing loss factor does have a correlation with the dry friction coefficient as $\gamma \sim 0.71 f$ at a rotational speed of 50 krpm. Since the top foils with VN or TiSiN are coated on both sides, kinetic friction between the back of a top foil and the bumps' crests likely lessens during sustained contact.

ACKNOWLEDGEMENTS

I thank Dr. Luis San Andrés, committee chair and advisor, for accepting me into the Tribology Group at Texas A&M University Turbomachinery Laboratory. I am truly grateful for his guidance and support, as well as for his prompt response and numerous revisions of my graduate work output (reports and thesis).

I acknowledge the U.S Navy and IBC Materials Company for their financial support.

Thanks to the staff of the Turbomachinery Laboratory for their technical assistance and advice. Finally, I thank the graduate students of the Turbomachinery Laboratory, in particular Bonjin Koo, Seunghwa Jeung, Travis Cable, Xulieng Lu, Yong Zheng, Tingcheng Wu, Behzad Abdollahi, Rasool Koosha, and Keith Gary for their encouragement, advice and friendship.

CONTRIBUTORS AND FUNDING SOURCES

Contributors

This work was supervised by a thesis committee consisting of Dr. San Andrés and Dr. Delgado of the Department of Mechanical Engineering and Dr. Hurlebaus of the Department of Civil Engineering.

All work for the thesis was completed independently by the student.

Funding Sources

This work was made possible in part by the U.S Navy and IBC Material Company under TEES project 506480 0001.

Its contents are solely the responsibility of the authors and do not necessarily represent the official views of the U.S Navy and IBC Material Company.

NOMENCLATURE

$a_{X(t)}, a_{Y(t)}$	Bearing accelerations along X and Y directions [m/s^2]
$\overline{A}_{X(\omega)}, \overline{A}_{Y(\omega)}$	DFT of bearing accelerations along X and Y directions [m/s^2]
$C_{S\alpha,\beta}$	Squirrel cage equivalent damping coefficients [Ns/m] ; $\alpha, \beta = X, Y$
$C_{\alpha\beta}$	Equivalent damping coefficients[Ns/m] ; $\alpha, \beta = X, Y$
D	Shaft (journal) diameter, D=2R [mm]
D_i	Bearing inner diameter [mm]
D_o	Bearing outer diameter [mm]
f	Drag friction coefficient [-] ; $f=T/(RW)$
f_o	Bearing dry-sliding friction coefficient [-] ; $f_o=T_o/(RW)$
F_X, F_Y	Applied excitation force along X and Y directions [N]
$\overline{F}_{X(\omega)}, \overline{F}_{Y(\omega)}$	DFT of excitation forces along X and Y directions [N]
F_A	Applied static load [N]
$H_{\alpha\beta}$	Bearing complex stiffness coefficients [N/m] ; $H_{\alpha\beta} = K_{\alpha\beta} + j\omega C_{\alpha\beta}$, $\alpha, \beta = X, Y$
h_B	Bump foil strip height [mm]
j	Imaginary number, $\sqrt{-1}$.
$K_{S\alpha,\beta}$	Squirrel cage stiffness coefficients [MN/m] ; $\alpha, \beta = X, Y$
$K_{\alpha\beta}$	Bearing stiffness coefficients [MN/m] ; $\alpha, \beta = X, Y$
k	Spring constant [N/m]
L	Bearing axial width [mm]
L_T	Torque arm length [mm]
l_0	Bump foil strip length [mm]
M_B	Bearing mass [kg]
M_S	System (Bearing + squirrel cage) mass [kg]
N_B	Number of bumps [-]

p	Bump foil strip pitch [mm]
R	Shaft (journal) radius [mm]
T	Bearing drag torque [Nmm] ; $T = \delta \times k \times L_T$
T_o	Dry-sliding friction torque [Nmm]
t	Time [s]
t_T	Top foil thickness [mm]
t_B	Bump foil strip thickness [mm]
W	Net static load [N] ; $W=F_A-W_B$
W_B	Bearing weight [N]
X,Y	Coordinate system [m]
x, y	Absolute bearing displacement [mm]
x_j, y_j	Absolute journal displacement [mm]
x', y'	Bearing displacement relative to the journal [mm]
$\bar{x}'_{(\omega)},\bar{y}'_{(\omega)}$	DFT of bearing relative displacements [mm]
γ	Bearing material loss factor [-] ; $\gamma=\omega(C_{XX}+C_{YY})/(K_{XX}+K_{YY})$
$\bar{\gamma}$	Average loss factor [-] ; $\bar{\gamma}=\frac{1}{\omega_2-\omega_1}\int_{\omega_1}^{\omega_2}\gamma\, d\omega$
Ω	Rotational speed [krpm]
ω	Excitation frequency [rad/s]

ACRONYMS

ACM	Air Cycle Machine
BFB	Bump Foil Bearing
DAQ	Data Acquisition System
FB	Foil Bearing
GFB	Gas Foil Bearing
PS	Plasma Sprayed
TC	Turbocharger

TABLE OF CONTENTS

Page

LIST OF FIGURES

Page

LIST OF TABLES

Page

CHAPTER I

INTRODUCTION

Gas Foil Bearings (GFBs) are cost-effective, simple to assemble and install, thus offering a remarkable advantage to high speed rotating machinery [1], such as in Air Cycle Machines (ACMs). GFBs fulfill most of the requirements of oil-free turbomachinery with operation at high temperature and high speed as well as enabling low drag friction, long operating life, and material damping for mechanical energy dissipation.

Figure 1 shows a schematic view of a generation I corrugated bump type foil bearing (BFB) comprised of one or more bump foil strip layers (under-spring structure) and a top foil, both elements secured into a bearing cartridge. The bearing support enables operation at high rotational speed with little drag friction. During operation, the rotor lifts off from the top foil surface at a certain speed, determined largely by the applied load and the low-friction characteristics of the solid lubricant coating the top foil. Once airborne, a gas BFB operates with a minute gas film that is extremely stiff when compared to the stiffness of the bump-strip layer.

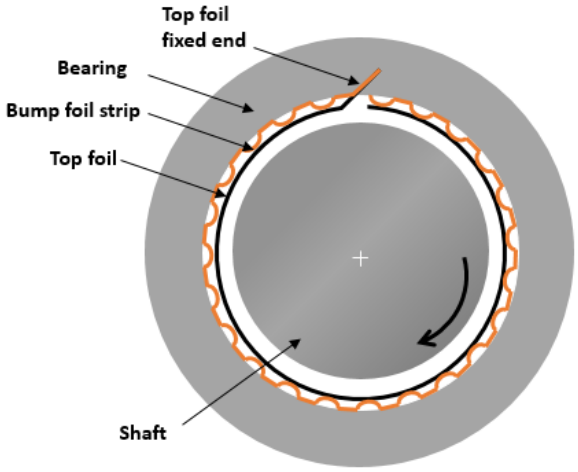

Figure 1. Schematic view of a corrugated bump-type GFB (Generation I).

Incidentally, BFBs are prone to show low frequency (sub-synchronous) whirl rotor motions due to the hardening characteristic of the under-spring structure [2,3]. These whirl motions, typically of large amplitude, have a frequency equal to the system natural frequency (a rigid body mode) and reach limit cycles. Often, rotors supported on gas BFBs operate for long periods of time with these limit cycles and do not affect the system reliability or its efficiency.

BFBs provide advantages such as low drag power loss, ability to tolerate mechanical imperfections (such as runout and static misalignment), as well as the ability to operate at high speed and high temperature and even with increasing levels of contamination. However, BFBs exhibit drag friction contact during rotor start and stop events, which can cause premature wear of both shaft and top foils. Thus, successful implementation of BFBs requires selection of an adequate protective coating for the top foil to ensure long life with minimal maintenance.

Comprehensive static and dynamic load tests are conducted to evaluate the performance of generation I type BFBs with both uncoated and coated top foils. Static load test results determine drag friction coefficients and lift-off speeds for the test bearings. In addition, rotordynamic test results provide rotordynamic force coefficients (stiffness and damping) and loss factors of the test bearings.

Literature review

Background

BFBs are typically categorized into three different types, termed as generations I, II, and III bearings. Chen et al. [4] and DellaCorte et al. [5] provide details on the characteristics of each BFB generation (different assembled geometries) and describe manufacturing procedures for a bump strip layer and top foil for generation I and II type bearings.

In 1953, Block and Van Rossum [6] introduced the basic concept of the first compliant foil bearing (FB). The authors noted that a large film thickness in a FB can aid to address issues of operation under stringent operating conditions (high temperature and high speed) by reducing the effect of thermal expansion for both the rotor and its bearing. Large film thicknesses in a FB also enable improved reliability and load capacity. Thus in the late 1960's, gas foil bearings (GFBs) became more widely used in aircraft ACMs [1]. More recently, GFBs have been researched for application in automotive turbochargers (TCs) [7,8], for example.

Coating materials for BFBs

The development of a wear-resistant, lubricious multi-layer coating able to withstand a wide operation range can significantly enhance the durability of a foil bearing for both an air platform and commercial turbomachinery applications. An inadequate choice of coating material can cause premature wear on both the journal and the top foil during start up and shut down events [9].

DellaCorte et al. (2004) [10] applied a solid lubricant coating on a test rotor (35 mm in a diameter) and top foil of a generation III BFB. The test bearings have a diameter of 35 mm and a length of 26 mm. The rotor surface is first coated with a NASA designed PS304®[1] coating and overcoated with polyimide or Molybdenum Disulphide (MoS_2). The top foil surface is coated with one of two coatings; aluminum bronze (Al-Cu), or sputtered alumina (Al_2O_3). Tests were performed to measure bearing load capacity at room temperature and with a journal rotation speed of 14 krpm (ΩR=26 m/s). The test results show that the combination of the PS304® coated rotor with a sacrificial layer (overcoated) of MoS_2 running against the Al-Cu coated top foil provides the maximum load capacity, when compared to the alumina based coating. The authors note that the application of an effective solid lubricant film, such as MoS_2, on the rotor or the top foil surface is necessary to achieve better performance upon initial installation.

Heshmat et al. (2005) [11] evaluate top foil coating performance for thrust BFBs at a high temperature (~810 ºC) and high operational rotor speed (~54 krpm, ΩR_{center}=204 m/s)

[1] PS: Plasma Sprayed. PS304® is a high temperature composite solid lubricant coating composed of Ni-Cr, Cr_2O_3, BaF_2-CaF_2.

under an applied specific load (*W/(LD)*) of 13.8 kPa. The Inconel X-750 top foils (inner and outer radii of 23.5 mm and 48.5 mm, respectively, and a thickness of 0.15 mm) are coated with several types of Korolon™ coatings for tests conducted with a high temperature high speed tribometer[2]. The test results demonstrate that Korolon™ coatings show remarkable tribological characteristics, and a small dry-sliding friction coefficient (less than 0.1) during rotor start up and shut down events. The physical properties of the Korolon™ coating are highly affected by temperature during the tests.

Jahanmir et al. (2009) [12] investigate the performance characteristics of coatings for thrust BFB applications. The test bearing has an inner radius of 23.5 mm and an outer radius of 48.5 mm. Tests were performed at room temperature (20-25 ºC) with a rotor speed of 10 krpm (ΩR_{center}=40 m/s) and under an applied specific load of 14 kPa (10 N) on the test bearing. The test coatings include a tungsten disulfide-based solid lubricant, hydrogenated diamond-like carbon film (H-DLC), and thin dense chrome plating. From the various combinations tested, the top foil coated with the tungsten disulfide-based solid lubricant and the collar coated with either chrome-plated or H-DLC-coated show a lower coefficient of friction than that for an uncoated top foil and collar; and after testing, exhibit less wear than the elements without coating. The test results show the best tribological performance occurred with a combination of a soft (polymer based) coating for the top foil and a hard, wear resistant coating for the collar.

Kim and Zimbru (2012) [13] present test results for dry-sliding friction characteristics

[2] A tribometer is used to evaluate the tribological performance (coefficient of friction, friction force, etc.) of materials using a pin-on-disk, ball-on-disk, or a pad-on disk configuration. In this case, the tribometer was used in a pad on disk configuration.

of a hybrid air FB during rotor start up and shut down events, as well as the bearings' thermal behavior at rotor speeds below 10 krpm (ΩR=53 m/s). The hybrid (hydrostatic and hydrodynamic) air FB has a diameter of 101.6 mm, a length of 82.6 mm with a corrugated bump foil and a Teflon coated top foil. The authors perform tests to measure the drag torque under a range of applied specific loads, 27.4 - 48.8 kPa. Results show clear wear marks on portions of the coated top foil as the rotor had eroded the Teflon coating. The authors note that these rubbing contacts are unavoidable for FBs due to the variability in their construction (i.e., bump height, foil thickness and coating thickness variations). The locations of the wear marks indicate areas where the foil bearing is not uniform, thus evidencing first points of contact during rotor start up and shut down events.

Aouadi et al. (2014) [14] review recent literature on coatings that could replace solid lubricants at high temperature (~650 ºC). Lubricious oxides can help to reduce unnecessary wear from dry-sliding friction at high temperature operation. In air FB applications, the authors note that, for proper operation, the wear of the top foil must not exceed 25% of its initial thickness. Thus, thermal stability is a foremost requirement, which prompted NASA to develop several coating to address this issue. The PS300® coating provides low temperature lubrication as well as a dry-sliding friction coefficient of ~0.3 for operation from room temperature to 650 ºC. Most recently, the PS400® coating, with similar components as in PS300®, was developed to avoid oxidative effects causing dimensional swelling.

DellaCorte et al. (2014) [15] evaluate a PS400® coating on a rotor used in a commercial oil-free microturbine engine (30 kW). The coating characteristics and its

durability are estimated from a cold start and a hot shut down events, during multiple 12 hour operation, once per a day, with a hot rotor spinning of 96 krpm (ΩR=160 m/s), and at an environment temperature of ~500 ºC. After 2,200 cycles of start-up and shut down events, the color of the rotor surface coated with the PS400® had changed from a metallic silver to a dark grey with a polished surface, thus indicating a good tribological performance as well as an ideal surface for a rotor. No wear on the rotor was found from a measurement of the shaft diameter. The authors note that the PS400® coating is reliable regardless of high temperature variations; its friction and wear resistance are comparable to those of PS304® coating at ambient temperature, while significantly improving at an elevated temperature, in particular for wear.

Zywica et al. (2016) [16] present research on an antifriction coating for BFBs, and focus on the temperature distribution evaluated with thermocouples and a thermovision camera. The test bearing, 35 mm in diameter and 40 mm in length, has three separate bump foils placed along the bearing cartridge circumference. The base material for the top foils is Inconel with a polymer coating (AS20); whereas a chromium oxide (Cr_2O_3) is applied on the journal surface by a plasma spraying technique. The test results shows that a peak torque of 120 N-mm occurs when the rotor touches the bearing, and an airborne torque of 10 N-mm for operation at a speed of 21 krpm (ΩR=38 m/s). The test results also demonstrate a satisfactory level of wear resistance after 10,000 start/stop cycles.

Radil and DellaCorte (2016) [17] evaluate PS400® coating for high temperature application up to 927 ºC by performing tests with uncoated top foils loaded against a PS400® coated shaft. The PS400® coating was initially engineered to reduce the wear

during rotor start and stop events in FBs, but further to work in a high temperature environment (>250 ºC) where dry-sliding friction and wear may cause problems. The test results show dry-sliding friction coefficients of the coating from 0.37 to 0.84 at 260 ºC to 927 ºC, where the coating became thermally unstable. The results also indicate that PS400® can provide appropriately a protective solid lubricant for low speed range and high temperature condition with low surface wear and friction coefficients. The authors note that the coating can generate a lubricious black oxide marks on the coated surface thus indicating a constant contact. The absence of marks between the coated surface and the rotor evidence that the coating can withstand large contact stresses.

Sim and Park (2017) [18] perform measurements of the static and dynamic characteristics of a generation I BFB whose bump foil is in series with a soft polymer layer. The authors test three bearing configurations, comprising of a normal GFB, a gas polymer bearing (GPB), and gas foil-polymer bearings (GFPB), each with a diameter of 40 mm and a length of 35 mm. A top foil for the test bearing is coated with a MoS_2 coating (thickness ~20 μm) to reduce friction torque during rotor start and stop events. Static load versus deflection test results show nearly identical clearances and behavior for the three different bearings, each displaying the typical nonlinearity in hysteretic damping. In addition, dynamic load tests show that both the GPB and GFPB have higher material loss factors than the GFB. For an excitation range from 300-800 Hz, the GPB shows superior damping capability, with a loss factor of $\gamma \sim 0.2$, compared to the GFB with $\gamma \sim 0.1$ and the GFPB with $\gamma \sim 0.15$. Rotordynamic tests on a dedicated test rig show that the lower

structural stiffness and higher structural damping of GFPBs can provide more bearing load capacity and rotordynamic stability at high speed operation.

Recently, studies on rotor coatings for application at high temperature (>250 ºC) have been actively conducted [14,15,16,17]. Therefore, further research on top foil coating is necessary to provide more empirical data. Tests conducted at room temperature (20 ºC) could be a cornerstone to step over to high temperature experiments.

Drag torque measurements

In hydrodynamic foil bearings without jacking pressure ports, the rotor is typically in contact with and rests on the smooth top foil at start up. The rotor comes again into solid contact during a shut-down event. Dry-sliding friction contact consequently causes a significant power loss on any rotor system with GFBs. Thus, to ensure long bearing life, it is important to reduce the rotor lift-off speed and torque during start-up/shut-down events.

San Andrés and Chirathadam (2012) [19] perform static and dynamic load tests to compare the characteristics of two different types of FB of similar size, 36.5 mm in diameter and 38.1 mm in length. The tests report measured lift off speed and torque, bearing structural stiffness, as well as rotordynamic force coefficients. The authors note that the maximum drag torque increases with an increase in applied static load, and that the power loss of a BFB increases with an increase in rotor speed and applied static load.

Ryu and San Andrés (2013) [20] highlight the importance of cooling flow for GFB operation at high temperature. They conduct tests with a generation II BFB (diameter of

38 mm and length of 25.4 mm) and a hollow shaft heated by an electric cartridge heater. During operation with a rotor speed of 37 krpm (ΩR=134 m/s), the test bearing (closest to the heater) seized at a shaft temperature of ~250 ºC. The rotor stopped abruptly as a result of inadequate thermal management (no cooling air). A rapid raise of the test bearing (and rotor) temperature caused a reduction in radial clearance, leading to increased drag torque (and gas temperature raise), and eventual solid contact between the rotor and top foil. Thus, sustained dry-sliding friction contact between the rotor and the top foil lead to the bearing failure (top foil melted). A post-inspection test of the failed bearings shows that there was enough frictional induced heating to weld the top foil to the bump foil crests. The authors recommend supplying abundant pressurized air to implement GFBs at high temperature for proper thermal management.

San Andrés and Norsworthy (2016) [21] perform measurements characterizing the static and dynamic load performance of a generation I BFB. The test bearings have a diameter of 36.5 mm and a length of 38.1 mm, and are constructed with shims of thickness equal to 30 μm and 50 μm. The shaft is coated with a thin chrome layer of ~25 μm in thickness. In the tests, drag torque measurements during rotor acceleration tests show a large dry-sliding friction coefficient for the bearing with shims. Hence, the dry-sliding friction coefficients of a shimmed bearing is a larger in magnitude than that of the original bearing. Thus, the shimmed BFB needs more torque to initiate its operation. Once airborne, the test BFBs, without and with shims, show almost identical low friction coefficient.

Ryu et al. (2017) [22] conduct experiments on both oil-free (air-lubricated) TC and oil-lubricated TC (with identical compressor and turbine wheels) to compare drag friction

and acceleration torque during rotor start up and shut down events. The test bearing, with a diameter of 24.5 mm and a length of 19 mm, consists of a top foil and multiple bump strip segments. During a rotor speed up event (acceleration), the test results show that the drive torque for the oil-free TC rotor is larger than that for the oil-lubricated TC rotor due to the large mass and moment of inertia of the oil-free TC rotor. Above 20 krpm, the rotor speed for both TCs (oil & air lubricated) dramatically drops due to a viscous drag effect. When the rotor speed diminishes, the test results show that viscous drag coefficient and drag torque of both the oil-free and oil-lubricated TCs are almost identical. During operation without a forced cooling flow, the temperature of the test BFB increases up to ~70 ºC. In a post-test inspection, the rotor coated with PS400® shows neither wear nor significant scratches, thus indicating no rubbing contact between the rotor and the top foil.

Structural and rotordynamic force coefficients

Bearing dynamic force coefficients (stiffnesses and damping) play an important role on the rotordynamic response and stability of rotating turbomachinery. The maximum applied specific load (*W/(LD)*) is 144 kPa for a generation I BFB in Ref. [23].

San Andrés and Norsworthy (2013) [23] perform static load versus deflection tests to identify a BFB structural stiffness and a loss factor with a shimmed BFB. The test bearing, a generation I BFB with shims, has a diameter of 36.5 mm and a length of 38.1 mm. Under an applied static load of ~144 kPa (200 N), the structural stiffness of the bearing with shims shows a much higher magnitude than that of the bearing without shims. The tests results also reveal that the loss factor increases with an increase in preload by shimming.

Lee et al. (2013) [24] perform feasibility tests for an oil free TC supported on BFBs. Two test BFBs have a diameter of 24 mm and lengths of 25.3 mm (long) and 16.8 mm (short). Three metal shims inserted underneath the bump strip layers produce a mechanical preload. The tests evaluate the rotordynamic performance of an oil free TC through on-road tests with a diesel passenger vehicle, which is replaced the original floating ring bearing TC with the test BFB TC. Predicted force coefficients show larger direct stiffness and damping coefficients for the shimmed BFB than an original BFB (no shims), thus evidencing the influence of the mechanical preload. In addition, the shimmed BFB also shows an increased ratio of direct stiffness to cross-coupled stiffness, thus indicating an improvement of the bearings' rotordynamic performance.

Feng et al. (2015) [25] perform static and dynamic load tests to estimate the structural stiffness and equivalent viscous damping coefficient of a prototype multi-cantilever foil bearing (MCFB). The test MCFB has a diameter of 33.3 mm and a length of 26 mm, with a top foil supported by foil strips that multiple columns of compliant cantilevers are arrayed neatly to provide structural stiffness and mechanical damping. The test results show that the bearing stiffness and damping decrease with an increase in motion amplitude, and a large misalignment of a rotor can cause larger static and dynamic bearing stiffness as well as a larger equivalent viscous damping.

Feng et al. (2015) [26] investigate the effect of rotor misalignment on the static and dynamic performance of a generation I BFB. The test bearing has a diameter of 29.8 mm and a length of 30 mm, a top foil made of SUS304, and a shaft is polished without a coating. The static test results show that the BFB stiffness increases with a decrease in

clearance and an increase in misalignment angle. The dynamic load test results indicate that the dynamic stiffness, which largely depends on excitation frequency and rotor motion amplitude, slightly increases with an increase in excitation frequency and without shaft misalignment. When the rotor has a large misalignment angle, the dynamic stiffness decreases with an increase in excitation frequency, thus indicating that most bumps slip. Consequently, the dynamic stiffness and damping of BFBs increase with an increase in rotor misalignment angle.

Statement of work

Despite of their many advantages, BFBs have issues of dry-sliding and wear during critical moments of their operation. Specifically during rotor start and shut down events, the rotor contacts the top foil at a low rotor speed. This event could lead to surfaces' damage. In order to prevent premature wear of the BFB top foil, the proper selection and application of a protective coating is of importance to ensure long life with many start up and shut down events.

The main objective of the research is to characterize the static and dynamic performance of a bump type foil bearing with a diameter (D) of 36.5 mm and a length (L) of 38.1 mm, operating with uncoated and coated (VN, TiSiN, MoS_2) Inconel top foils. The drag friction coefficients of the test bearings under both dry-sliding and full hydrodynamic operation (airborne) are evaluated for operation under a static load from measurements of dry-sliding friction torque, lift-off shaft speed and torque, touch down shaft speed and

torque, and airborne torque. A bearing loss factor evidencing mechanical energy dissipation is obtained from further measurements of rotordynamic force coefficients for the test bearings dynamically excited over a range of excitation frequency. All tests are conducted at room temperature (20-22 ºC) in this research because of the limitation with the available hardware in the laboratory.

CHAPTER II

DESCRIPTION OF TEST BEARINGS AND THE EXPERIMENTAL FACILITY

Test bearings and the rotor

Figure 2 presents an assembled test bearing cartridge with a single top foil and bump under-spring layer and the test journal installed in a ball-bearing supported turbocharger (TC). A thin dense chrome coated journal (25 μm thick), connected to an air turbine, replaces the (original) compressor and its housing.

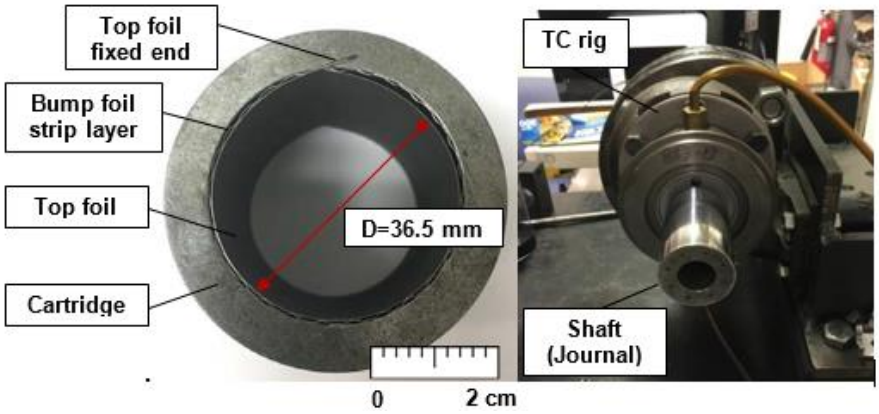

Figure 2. Assembled test BFB and journal installed in TC rig.

A typical BFB consists of a cartridge, an underspring bump-strip layer and an arcuate top foil. Figure 3 shows a photograph of three constructed foil bearings, one with an uncoated top foil and two with coated top foils. The underspring layers are identical for the three bearings. Table 1 lists the nominal dimensions of the assembled test bearings and Figure 4 shows a schematic view of a bump-strip layer and its geometric parameters.

Figure 3. Photograph of test bearings (Left : Uncoated, Center : TiSiN, Right : VN).

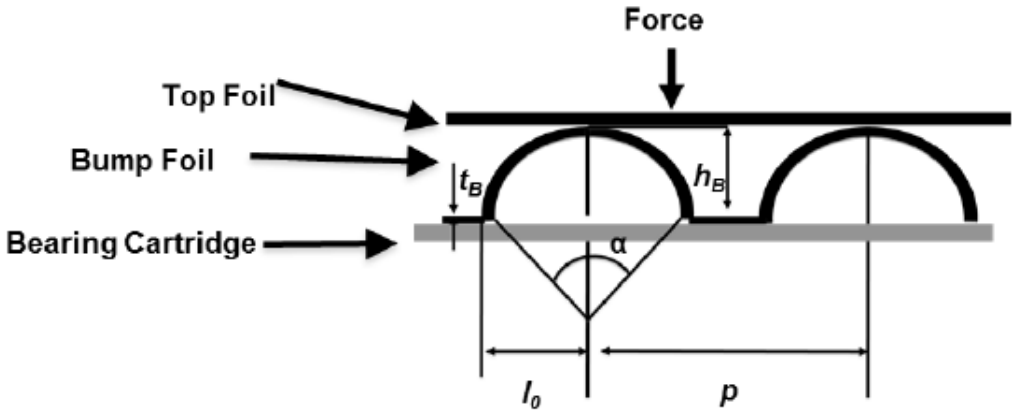

Figure 4. Schematic view of a bump foil and geometric parameters [27].

Table 1. Nominal dimensions of assembled test FBs. (Uncertainty: 0.005 mm)

Front and back of foil surface are coated except for the MoS_2 coated top foil (front only).

Cartridge	
Material	AISI 4140
Outer diameter, D_o	50.80 mm
Inner diameter, D_i	37.81 mm
Axial length	38.10 mm
Top foil	
Material	Inconel X-750
Width, L	38.10 mm
Length	120 mm
Thickness, t_T	0.127 mm
Coating thickness	VN coating ~5 µm
	TiSiN coating ~5 µm
	MoS_2 coating ~20 µm
Bearing clearance	Uncoated ~50 µm
(estimated)	VN coating ~40 µm
	TiSiN coating ~40 µm
	MoS_2 coating ~30 µm
Bump foil strip layer	
Number of bumps, N_B	27
Material	Inconel X-750
Bump width	38.10 mm
haf length, l_0	1.26 mm
thickness, t_B	0.127 mm
height, h_B	0.480 mm
pitch, p	4.400 mm
Shaft (Journal)	
Material	AISI 4140
Outer diameter, D=2R	36.50 mm

Drag torque measurements

Figure 5 depicts a schematic view of the test rig to measure the drag torque of a test bearing operating during rotor angular acceleration (start-up) and deceleration (shutdown) processes. Oil is continuously supplied to the turbocharger (TC) ball bearings throughout the tests. An inlet valve controls the delivery of air to the TC turbine to both accelerate and decelerate the rotor. An infrared tachometer mounted on the turbine discharge side measures the TC shaft rotational speed.

An ad-hoc feature of elastic ties wrapped around the bearing cartridge is assembled to apply a vertical load on the test bearing, while still allowing the bearing to rotate freely. The net static load (W) on the bearing equals the applied static load (W_S) minus the weight (W_B) of the bearing. During operation, journal rotation causes the lever arm to compress a calibrated spring. An eddy current sensor measure the deflection of the spring (δ), and the drag torque equals the product of δ times the spring constant (k ~ 8.9 N/mm) times the length of the arm lever (L_T ~ 170 mm) to the center of rotation ($Torque = \delta \times k \times L_T$).

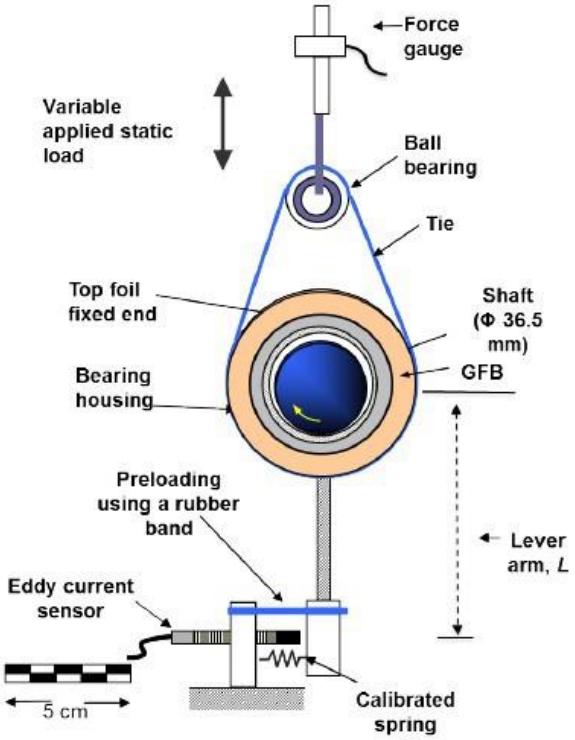

Figure 5. Schematic view of test rig to apply a static load and measure bearing drag torque [28]. Elastic tie and Lever arm equals to 170 mm in length.

Rotordynamic force coefficients tests

Figure 6 shows schematic views of the test rig to conduct dynamic load measurements. This configuration is a modified form of the rig used for the drag torque measurements. The test rig consists of a ball bearing supported TC capable of shaft speeds up to 100 krpm (see Figure 5). A squirrel cage, attached to a positioning table, supports the test bearing and helps to reduce misalignment of the bearing with respect to the journal during (static and dynamic) loading. Two orthogonally positioned shakers (45° away from the vertical plane) apply single frequency load excitations to the test bearing and the resulting motions

are recorded to extract the dynamic force coefficients. Two eddy current sensors record the bearing displacements relative to the shaft, two accelerometers (mounted to the bearing cartridge) measure absolute acceleration, and dynamic loads cells record the excitation forces along the *X* and *Y* directions.

An in house DAQ interface controls the (shaker) dynamic load characteristics (amplitude and frequency) while recording the bearing accelerations along two orthogonal directions, the bearing displacements relative to the spinning shaft, shaft speed and the applied dynamic loads.

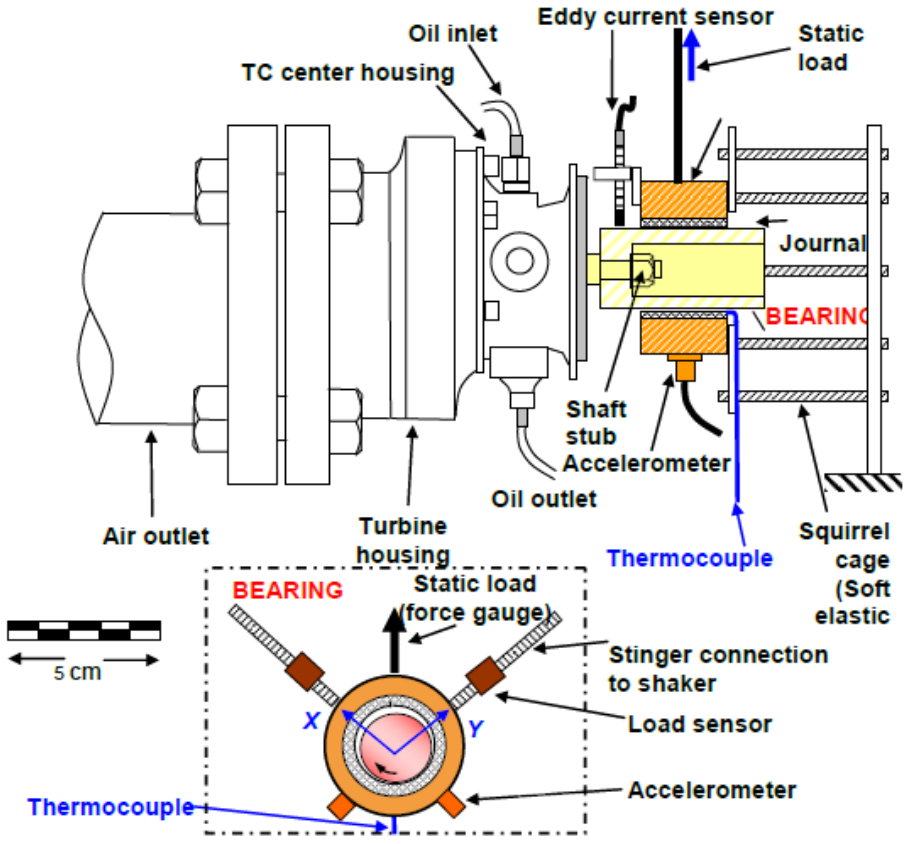

Figure 6. Schematic view of TC test rig setup for rotordynamics test [28].

CHAPTER III

MEASUREMENT OF DRY-SLIDING FRICTION TORQUE IN FOIL BEARINGS

Test procedure to measure the dry-sliding friction torque of test bearings

Figure 7 presents the setup for the measurement of dry-sliding friction torque while applying a static load on a test bearing. The bearing cartridge slides on top of a stationary journal. Both elements are located atop a table. During a test, the load gauge pulls on the bearing while the operator turns the shaft with a torquemeter and records the instance when the shaft or journal begins to turn.

Figure 8 depicts a schematic view of the static load applied on the bearing and that pushes it against the journal at a location 180º away from the top foil fixed end.

Using a torque screwdriver tool, one can determine the dry-sliding friction torque needed to overcome the static (dry) friction due to contact between the rotor and top foil. In the tests, the rotor is spun by hand with the tool while an ad-hoc setup applies a side specific load (6.4 – 25.6 kPa) onto the test bearing. At room temperature (20 - 22 ºC) under a dry environment condition, a measurement is repeated 10 times on each assembled BFB. The average torque magnitude and its uncertainty are presented.

A digital torque screwdriver, see Figure 9, has a resolution of 1 N-mm. The operator turns the screwdriver until the shaft turns inside the bearing. The instrument displays the maximum torque. After each test, the shaft is cleaned with alcohol and dried. Next, a second (and a third) bearing is inserted atop the shaft to repeat the measurement procedure.

The third coated bearing contains a top foil[3] coated with a layer of MoS_2 (0.15 mm thick).

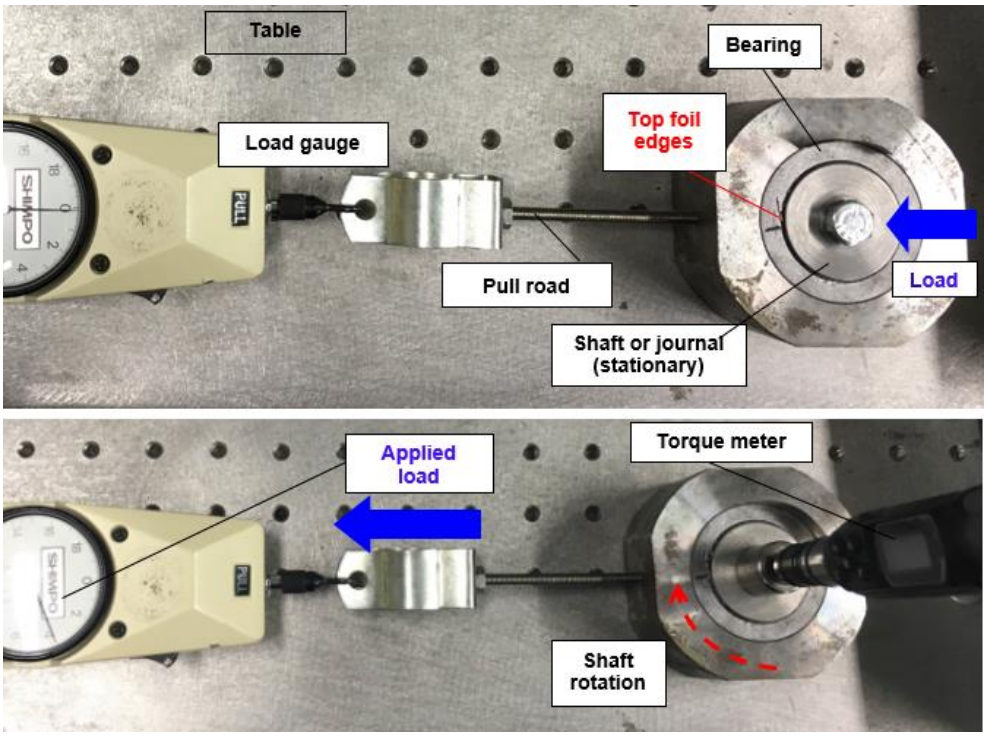

Figure 7. Setup for measurement of dry-sliding friction torque on a horizontal table. Static load applied on bearing with a dynamometer.

[3] The Korea Institute of Science and Technology (KIST) provided the top foils.

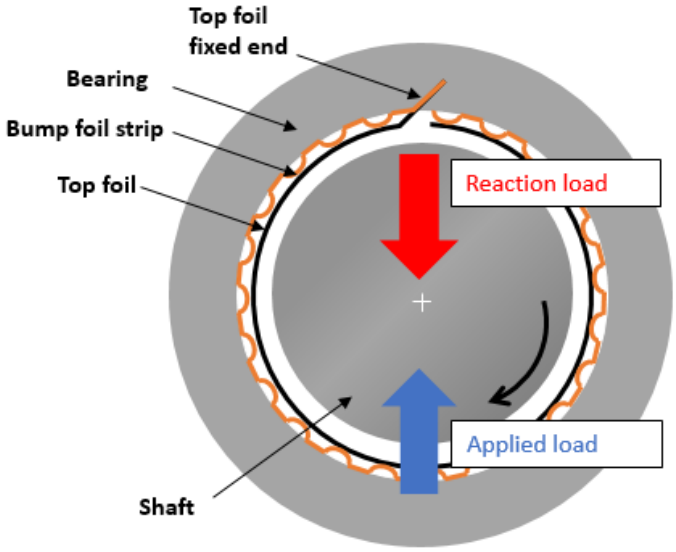

Figure 8. Schematic view of applied static load on bearing and reaction load from stationary journal.

Figure 9. Photograph of digital torque screwdriver.
(Range : 50-500 N-mm, Resolution : 1 N-mm, Accuracy : ±2% of CW, ±3% of CCW)

Dry-sliding (breakaway) friction torque measured by a digital torque screwdriver

Figure 10 shows views for a torque applied on the journal in a counter clockwise direction (against the fixed end of a top foil) and a clockwise direction (towards the free end of the top foil). In actual practice, the journal spins in the clockwise direction, i.e. from the fixed end towards the free end of the top foil.

Table 2 lists the measured dry-sliding friction torque (T_o) obtained with the digital torque screwdriver on one uncoated and three coated foil bearings. Table 2 also lists the applied load (W) divided by the projected area of the bearing[4] (LD), this is known as a specific load or pressure. The actual applied load (W) ranges from 8.9 N – 35.6 N (6.4-25.6 kPa). The dry-sliding friction torque (T_o) increases linearly with an increase in applied static load. The dry-sliding friction torque of the uncoated test bearing is lower than those for the bearings having the coated top foils. The bearing with a top foil coated with a VN layer shows the largest dry-sliding friction torque.

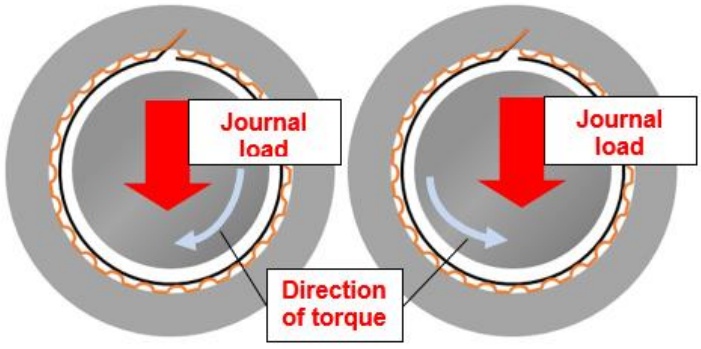

(a) Clockwise **(b) Counter clockwise**

Figure 10. Directions of applied torque and journal rotation.

[4] See the earlier Table 1 with dimensions. Nominal L=38.1 mm, and D=2R=36.5 mm

Table 2. Measured dry-sliding friction torque and friction coefficient for uncoated and coated test bearings conducted with a digital torque screwdriver. Average of 10 trials. (Uncertainty: 0.5 N-mm)

Clockwise direction (practice)

Specific load [kPa] *W/(LD)*	Dry-sliding torque [N-mm] and friction factor							
	Uncoated		TiSiN		VN		MoS_2	
	T_o	f_o	T_o	f_o	T_o	f_o	T_o	f_o
6.4	158	0.97	241	1.48	416	2.55	173	1.06
12.8	186	0.57	273	0.84	460	1.41	210	0.64
19.2	221	0.45	307	0.63	508	1.04	247	0.51
25.6	256	0.39	378	0.58	561	0.86	313	0.48

Counter clockwise direction

Specific load [kPa] *W/(LD)*	Dry-sliding torque [N-mm] and friction factor							
	Uncoated		TiSiN		VN		MoS_2	
	T_o	f_o	T_o	f_o	T_o	f_o	T_o	f_o
6.4	200	1.13	186	1.14	298	1.83	164	1.01
12.8	235	0.72	239	0.73	376	1.15	199	0.61
19.2	284	0.58	301	0.62	452	0.93	253	0.52
25.6	342	0.53	369	0.57	512	0.79	294	0.45

Dry-sliding friction factor of test bearings

The direction of shaft rotation affects the dry-sliding friction torque in a FB, as shown by the differences in magnitudes listed in Table 2. For applied torques clockwise, i.e. in the direction of rotor turning towards the free end of the top foil (as in practice), the coated test bearings show a larger dry-sliding friction torque than for the condition with a reverse direction torque. The opposite is true for the bearing with a bare (uncoated) top foil.

Figure 11 depicts the dry-sliding friction factor $f_o = T_o/(WR)$ versus specific load ($W/(LD)$) for each test FB estimated from the torque data listed in Table 2 for tests with

shaft turning clockwise and counter clockwise. The estimated f_o decreases as the specific load (*W/(LD)*) increases. The differences in friction coefficient vanish as the applied load increases. On the other hand, for a low specific pressure (~10 kPa), the friction factor differs considerably; the uncoated top foil bearing shows the lowest friction coefficient (likely because the absence of coating thickness increases the operating gap). As expected, journal rotation towards the top foil free end (clockwise) as in practice, gives a larger f_o than for shaft rotation in reverse. Note the friction factor $f_o > 1$ for a low specific load.

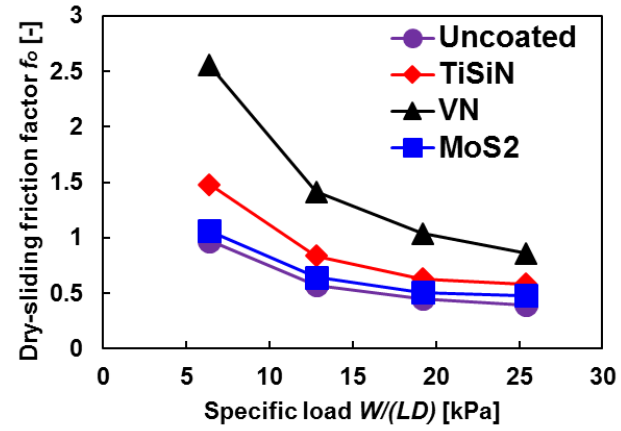

(a) Journal rotation clockwise (practice)

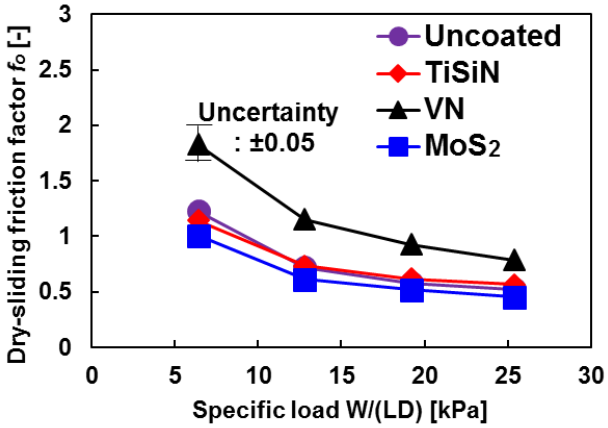

(b) Journal rotation counter clockwise

Figure 11. Dry-sliding friction factor of test foils versus specific load. Measurements with journal (hand) rotation in clockwise direction (*as in practice*) and counter clockwise.

Dry-sliding friction torque measurements conducted on TC test rig

Figure 12 depicts a schematic view of the TC test rig (reproduces Figure 5) to apply a static load and to measure the torque of a test bearing. The bearing is installed with the fixed end of the top foil upwards vertically. Note that the weight of the bearing assembly is 11.1 N. A torque screwdriver applies torque until the shaft with diameter D=36.50 mm turns inside the bearing. An ad-hoc DAQ code saves the displacement (δ) of an end rod pushing on a calibrated spring with stiffness k. The dry-sliding friction torque $T_o = k \times \delta \times L_T$ with L_T = 170 mm as the distance from the edge of the lever arm to the center of shaft rotation. The static load applied on each bearing ranges from 8.9–35.6 N (6.4-25.6 kPa). The measurements are conducted 10 times for each BFB and at room temperature under a dry environment condition. The shaft is cleaned with alcohol immediately after a test.

Figures 13 thru 15 depict the results of the dry-sliding friction (breakaway) torque measurements conducted on the TC test rig. Table 3 list the peak or maximum torque obtained from the graphs below.

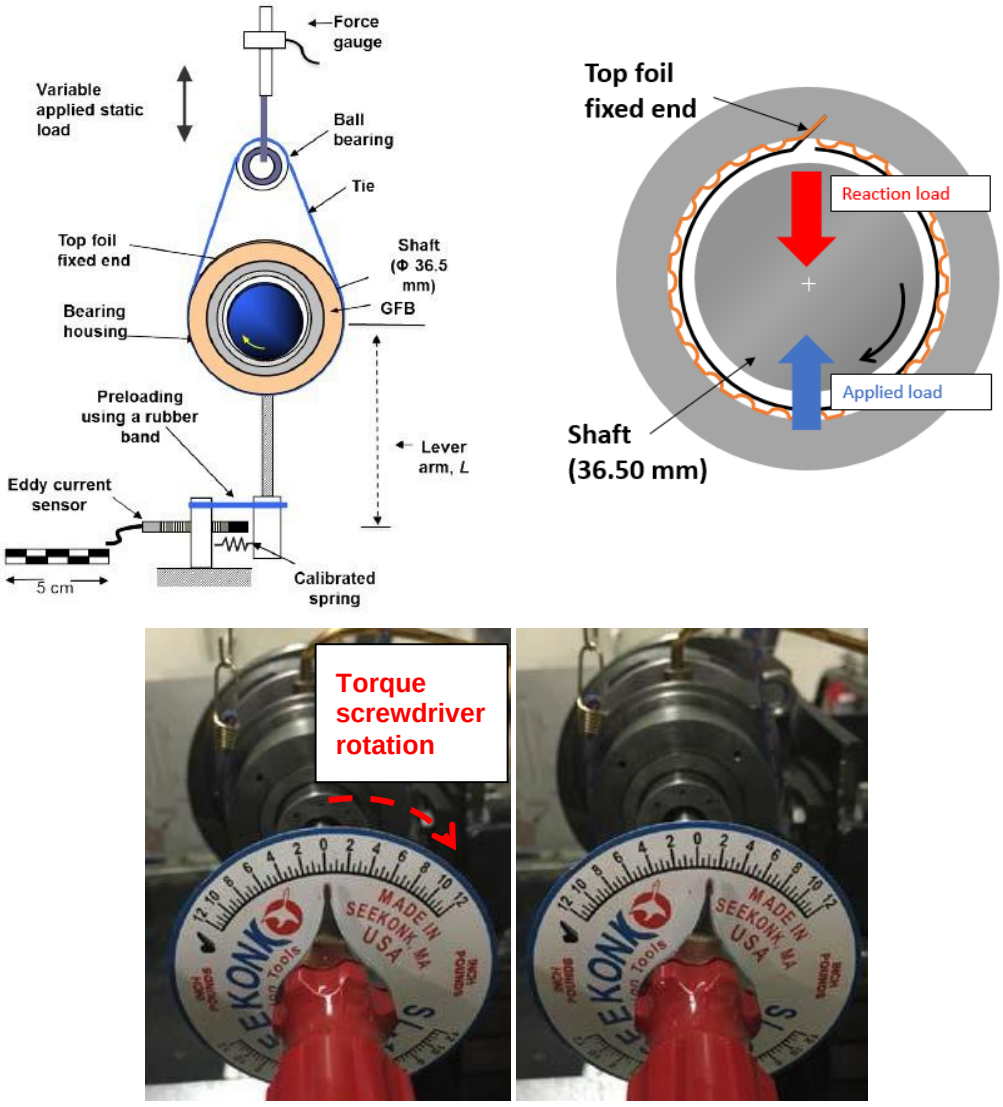

Figure 12. Schematic view of test rig [28] and torque screwdriver to measure the breakaway torque of the test bearing. Journal clockwise direction (rotor towards top foil free end).

Table 3. Measured dry-sliding friction torque and friction coefficient for uncoated and coated foil bearings conducted on TC test rig. Journal rotation in clockwise direction. Average of 10 trials. (Uncertainty: 1 N-mm)

Specific load [kPa] *W/(LD)*	Dry-sliding torque [N-mm] and friction factor							
	Uncoated		TiSiN		VN		MoS_2	
	T_o	f_o	T_o	f_o	T_o	f_o	T_o	f_o
6.4	141	0.87	211	1.30	436	2.69	139	0.86
12.8	168	0.52	273	0.84	487	1.50	193	0.59
19.2	228	0.47	311	0.64	530	1.09	208	0.43
25.6	276	0.43	390	0.60	589	0.91	298	0.46

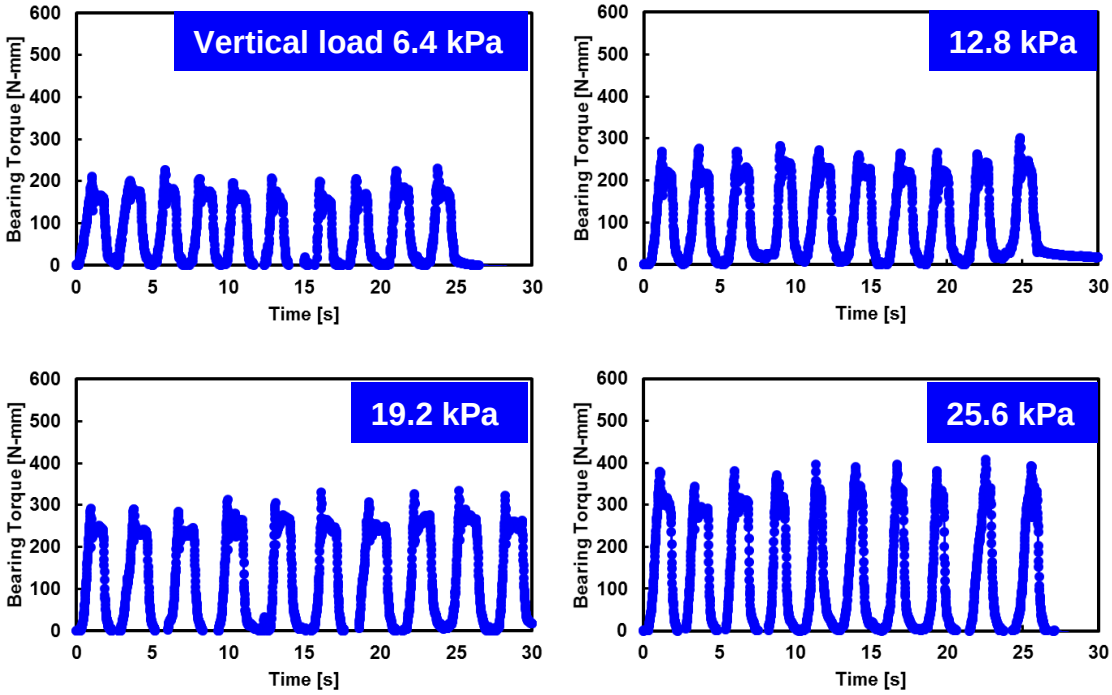

Figure 13. Dry-sliding friction torque on bearing with TiSiN coated foil. Vertical load varies 6.4 – 25.6 kPa (10 trials). Journal rotation in clockwise direction.

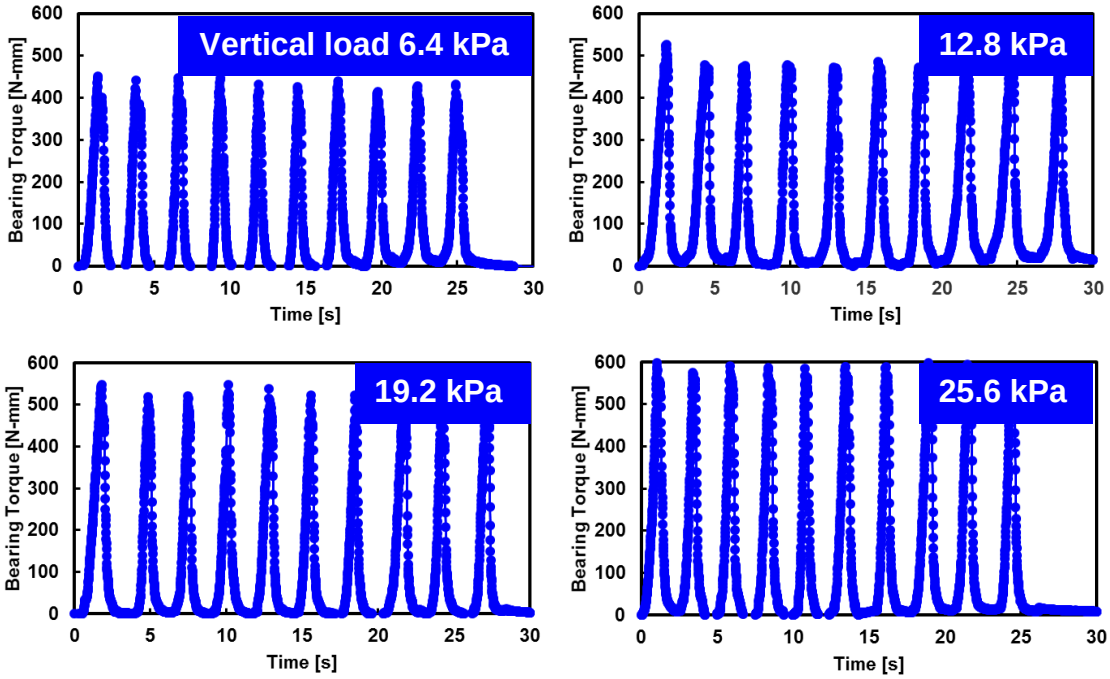

Figure 14. Dry-sliding friction torque on bearing with VN coated foil. Vertical load varies 6.4 – 25.6 kPa (10 trials). Journal rotation in clockwise direction.

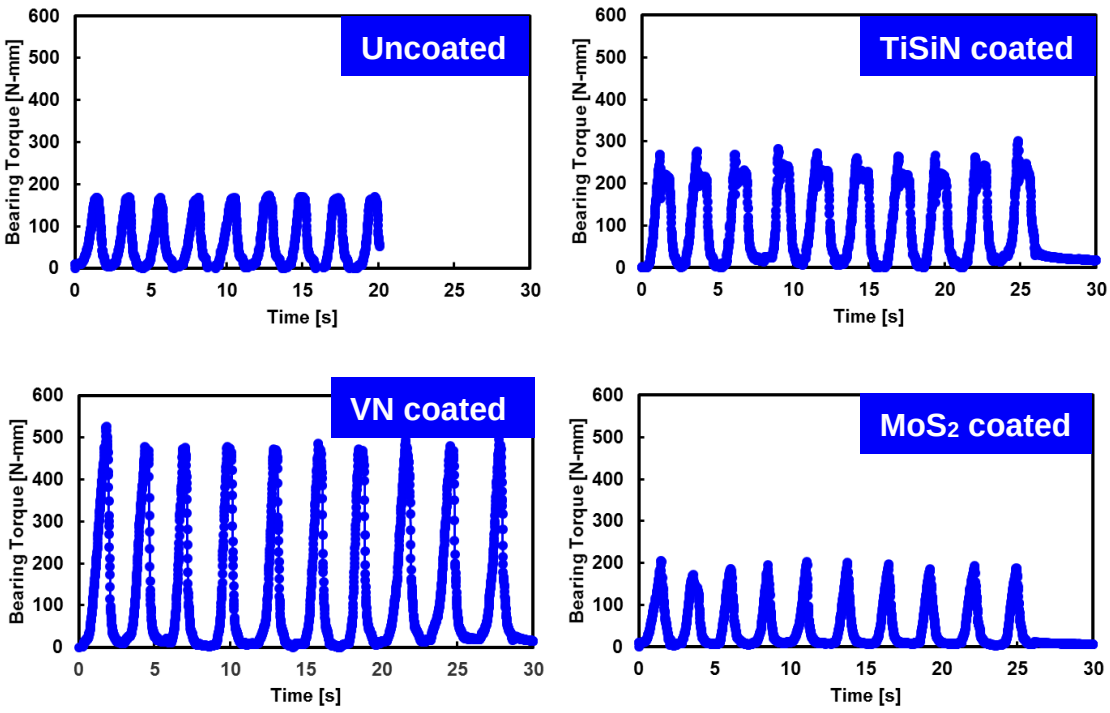

Figure 15. Dry-sliding friction torque on bearings with coated foils and uncoated foil. Vertical load= 12.8 kPa. (10 trials). Journal rotation in clockwise direction.

The results of the dry-sliding friction torque measurements conducted on TC test rig are very similar as the ones obtained with the digital torque screwdriver (Table 2 and Figure 11) and for a test bearing resting atop a horizontal surface (see Figure 7).

Among the test bearings, the bearing with a VN coated top foil shows the largest dry-sliding friction torque (f_o~2.69). The dry-sliding friction torque of the uncoated test bearing (f_o~0.87) is lower than those for the bearings having the coated top foils. This is because the absence of coating thickness increases the operating air gap, thus leading to a decrease in dry-sliding friction factor.

The dry-sliding friction factor derived from the drag torque decreases with an increase in an applied specific load. This is because the f_o decreases with an increase in an applied load W. The test results also indicate that the VN and TiSiN coated top foil bearings lead to larger energy loss than the MoS_2 coated top foil bearing.

CHAPTER IV

MEASUREMENT OF DRAG TORQUE IN FOIL BEARINGS DURING ROTOR ACCELERATION AND DECELERATION

Next, tests record the drag torque of a test BFB operating during rotor angular acceleration (start-up) and deceleration (shutdown) processes while the test bearing is under an applied load. To this end, a DAQ program recorded the shaft speed and torque (derived from calibrated spring) as well as the applied load and bearing and shaft temperatures.

Figure 16 shows drag torque versus rotational speed for a test bearing with TiSiN coated foil. The results are not consistent because there is unexpected axial movement of the foil causing rubbing contact which damage some of the test top foils, as depicted in Figure 17. Hence new foils (and test bearings) were built, see Figure 18, with set screws securing the foils (top and under-spring) to the housing and thus preventing their axial movement during operation.

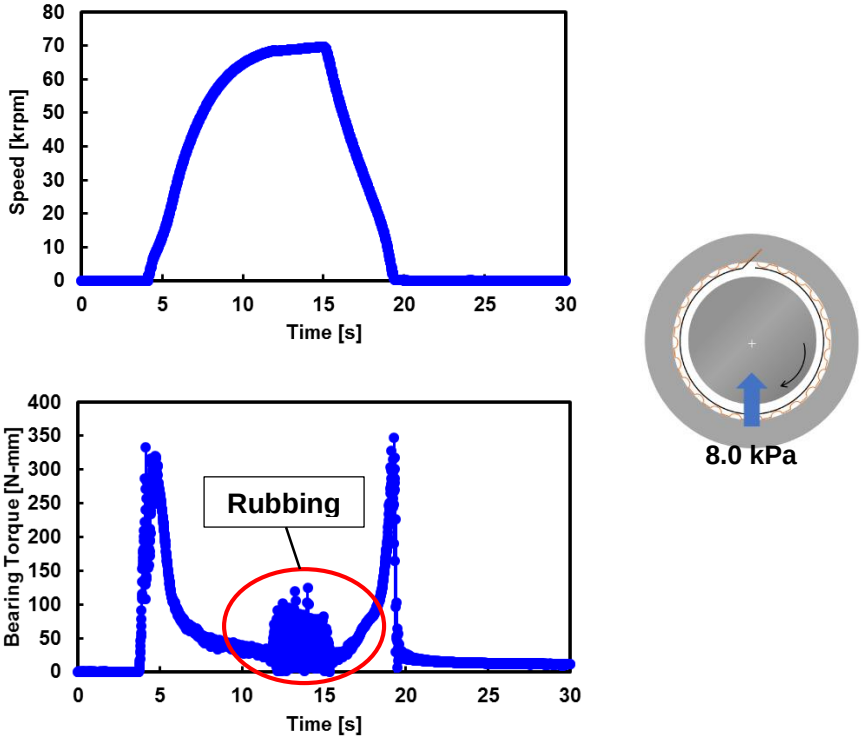

Figure 16. Recorded rotor speed and shear drag torque versus time. Operation with net specific load *W/(LD)* = 8.0 kPa. Bearing with TiSiN coated foil.

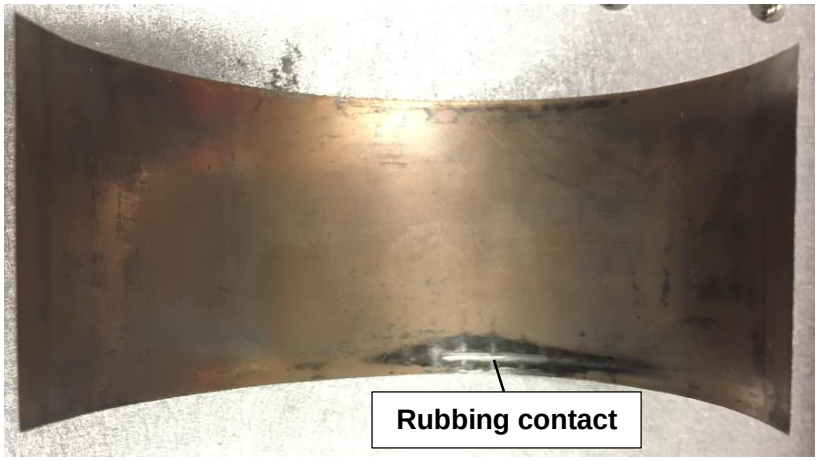

Figure 17. Evidence of rubbing contact and loss of coating on TiSiN coated top foil.

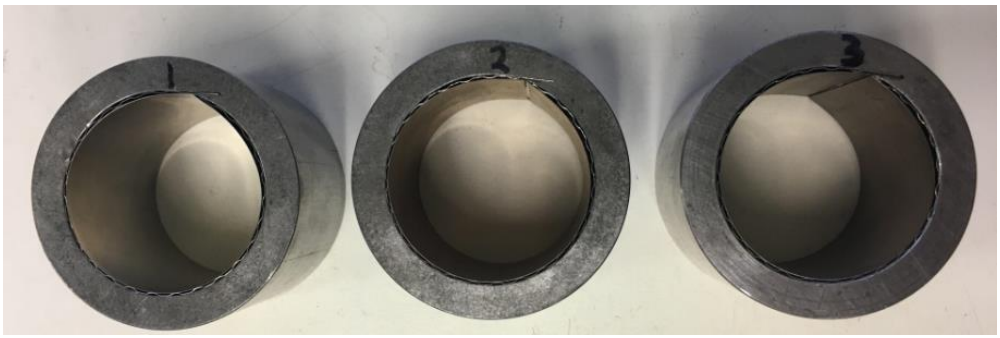

Figure 18. New (reconstructed) test bump foil bearings. Left : uncoated, Center and right: coated with TiSiN, VN.

Test procedure to measure the drag torque of test bearings during TC operation

Tests are performed in the TC driven test rig to measure the start-up and shut-down responses of the test FBs under distinct specific load conditions $W/(LD)$= -8.0 kPa, 0 kPa and 8.0 kPa. In a test, the operator opens the valve delivering pressurized shop air into the turbine of a TC. The TC rotor hosts a test FB and cartridge on the end that holds the TC compressor. The bearing is held in place by a soft structure, and a mechanism that prevents bearing rotation permits the measurement of the torque applied, see Figure 19.

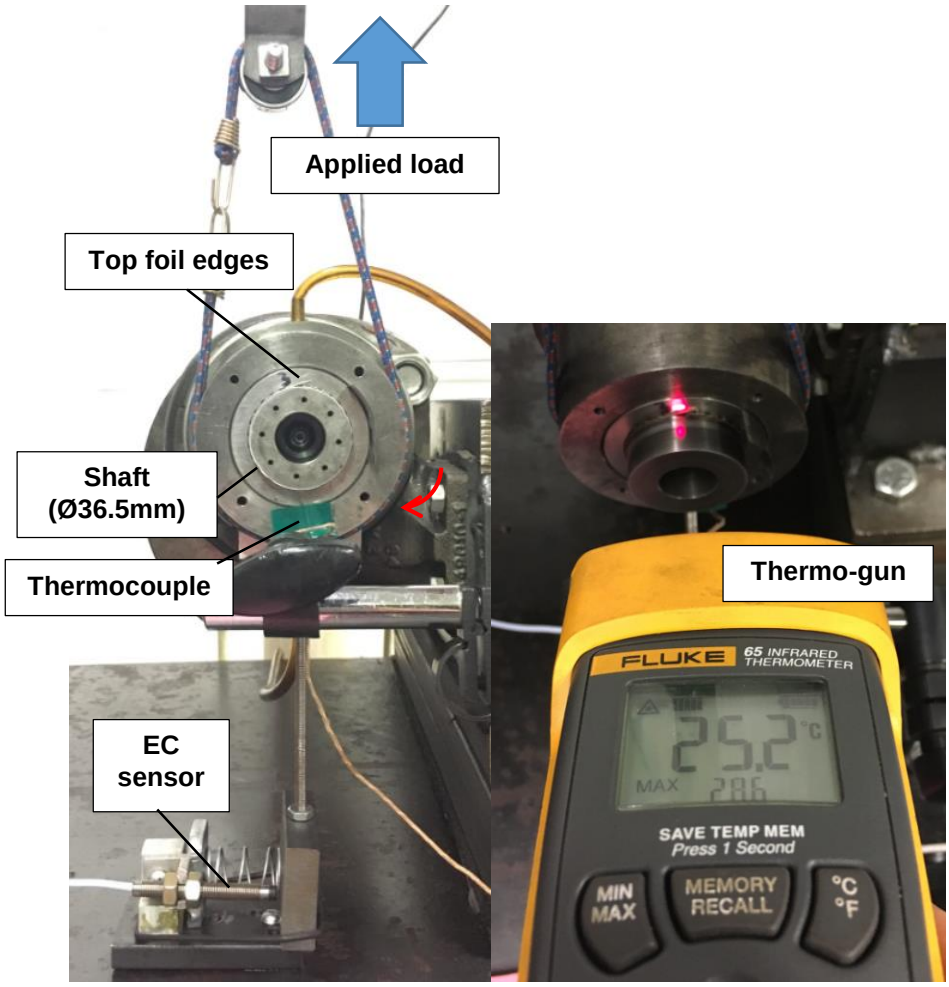

Figure 19. Photograph of TC test rig setup for the drag torque measurement.

The maximum rotor speed achieved in a test is 70 krpm (ΩR=134 m/s), and which happens ~20 s after the rotor begins to accelerate. Immediately after, the operator closes the air delivery valve and the rotor decelerates to rest. This event lasts about 5 s to 10 s. During an experiment, the rotor speed and torque are recorded. Other measurements include the temperature of the shaft and bearing cartridge using an infrared thermometer (thermo-gun) and a K-type thermocouple, respectively. The procedure calls for no less

than 10 start-stop tests, all conducted at room temperature (20 ºC) under a dry environment without humidity. Immediately after the last test, the test bearing is removed to visually inspect the condition of the top foil. The sequence for the tests is: VN coated FB → TiSiN coated FB → uncoated top foil → MoS_2 coated FB.

Foil bearings drag torque during rotor acceleration and deceleration tests

Figures 20 thru 22 show the rotor speed (top) and drag torque (bottom) versus time recorded for each test bearing for applied loads equaling -11.1 N (-1 W_B), 0 N (0 W_B), and 11.1 N (+1 W_B), respectively. The measurements reveal two regions of large drag torque at a typically low rotor speed; one happens during the rotor acceleration (start-up), and the other during shut down as the rotor decelerates to a quick stop. These regions of high torque reveal mainly the dry-sliding friction between the top foil and the rotor surface. A dramatic drop in drag torque indicates the rotor lifts off to operate airborne, i.e. with a minute air film separating the rotor from the top foil.

Once airborne, the torque albeit small is at times negative likely due to intermittent noise of the soft support structure.

Table 4 lists the recorded peak drag torque during startup (rotor acceleration) and shut down (rotor deceleration) for the four test BFBs operating with a static specific load *W/(LD)*= -8.0, 0, and 8.0 kPa. In general, the bearings with a coated top foil have a lesser drag torque than that with the uncoated top foil. Among the coated FBs, the bearing with VN coating shows the highest drag torque, whereas the one with MoS_2 shows the lowest torque. The drag torque recorded during a deceleration test is usually higher than that during the start-up process.

Table 4. Peak drag torque recorded during startup and shut down conditions. Four BFBs (one uncoated and three coated). Operation with net specific load *W/(LD)* = -8.0 kPa, 0 kPa, 8.0 kPa. Average of 10 trials. (Uncertainty: ±1N-mm)
Bearing weight W_B= 11.1 N. Load =W = $(F_A - W_B)$, L=38.1 mm, D_i=36.5 mm

Specific load [kPa] *W/(LD)*	Peak drag torque [N-mm]							
	Uncoated		TiSiN		VN		MoS_2	
	Start up	Shut down	Start up	Shut down	Start up	Shut down	Start up	Shut down
-8.0	176	160	102	144	116	150	74	91
0	70	93	60	73	66	130	51	83
8.0	170	191	111	175	124	155	80	84

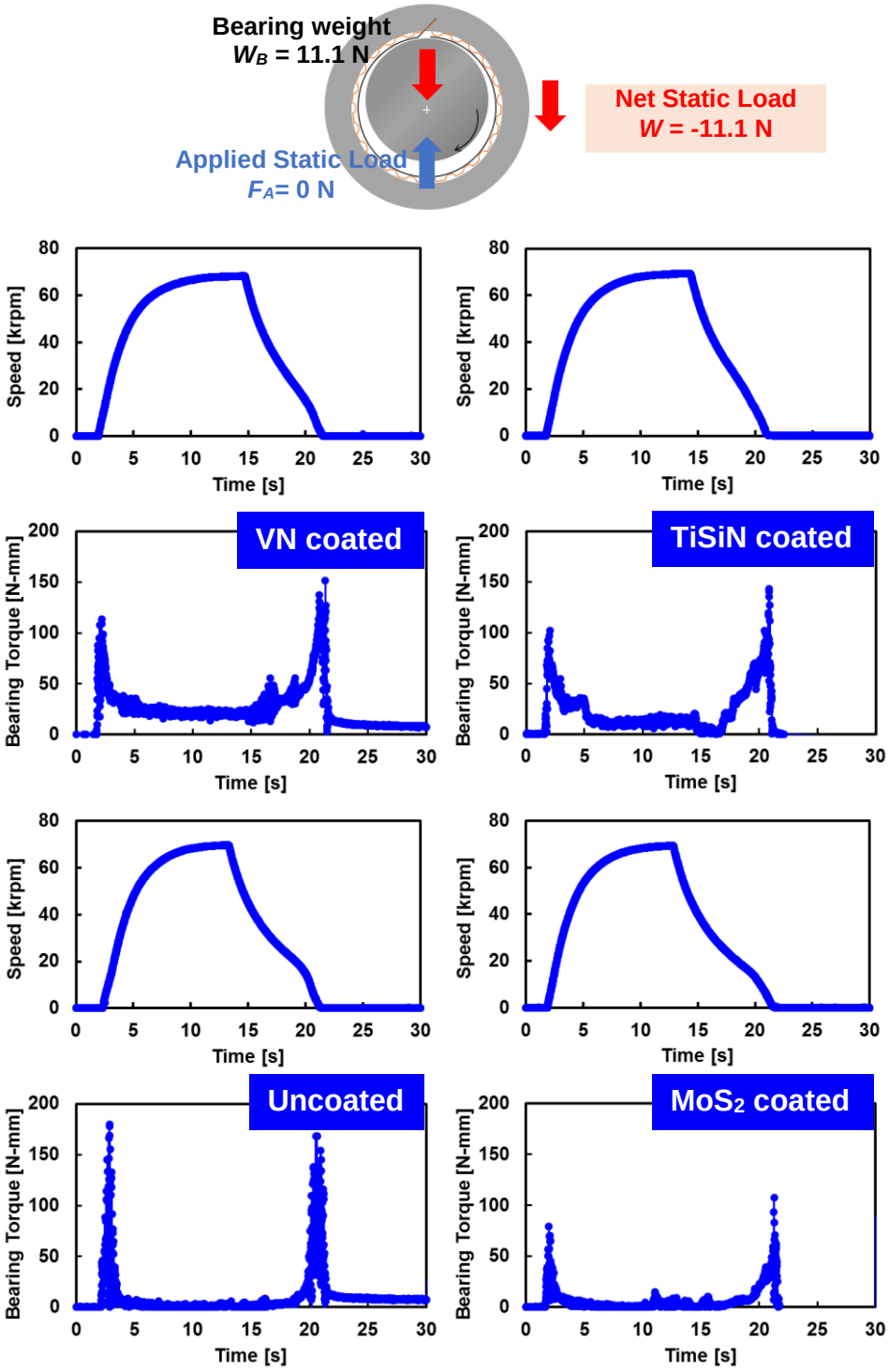

Figure 20. Recorded rotor speed and shear drag torque versus time. Four BFBs (one uncoated and three coated). Operation with net specific load *W/(LD)* = -8.0 kPa. Sample result from 10 trials.

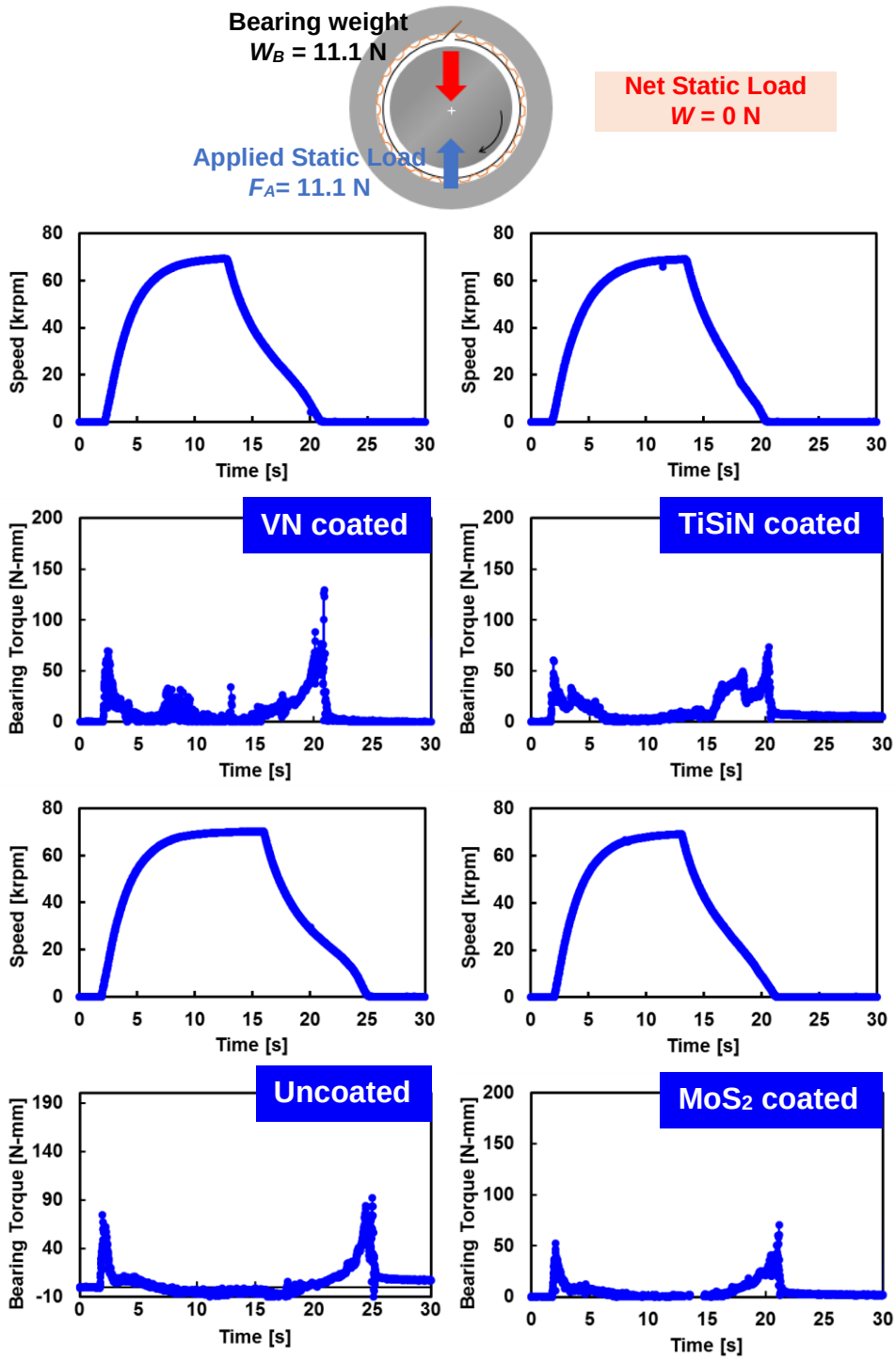

Figure 21. Recorded rotor speed and shear drag torque versus time. Four BFBs (one uncoated and three coated). Operation with net specific load *W/(LD)* = 0 kPa. Sample result from 10 trials.

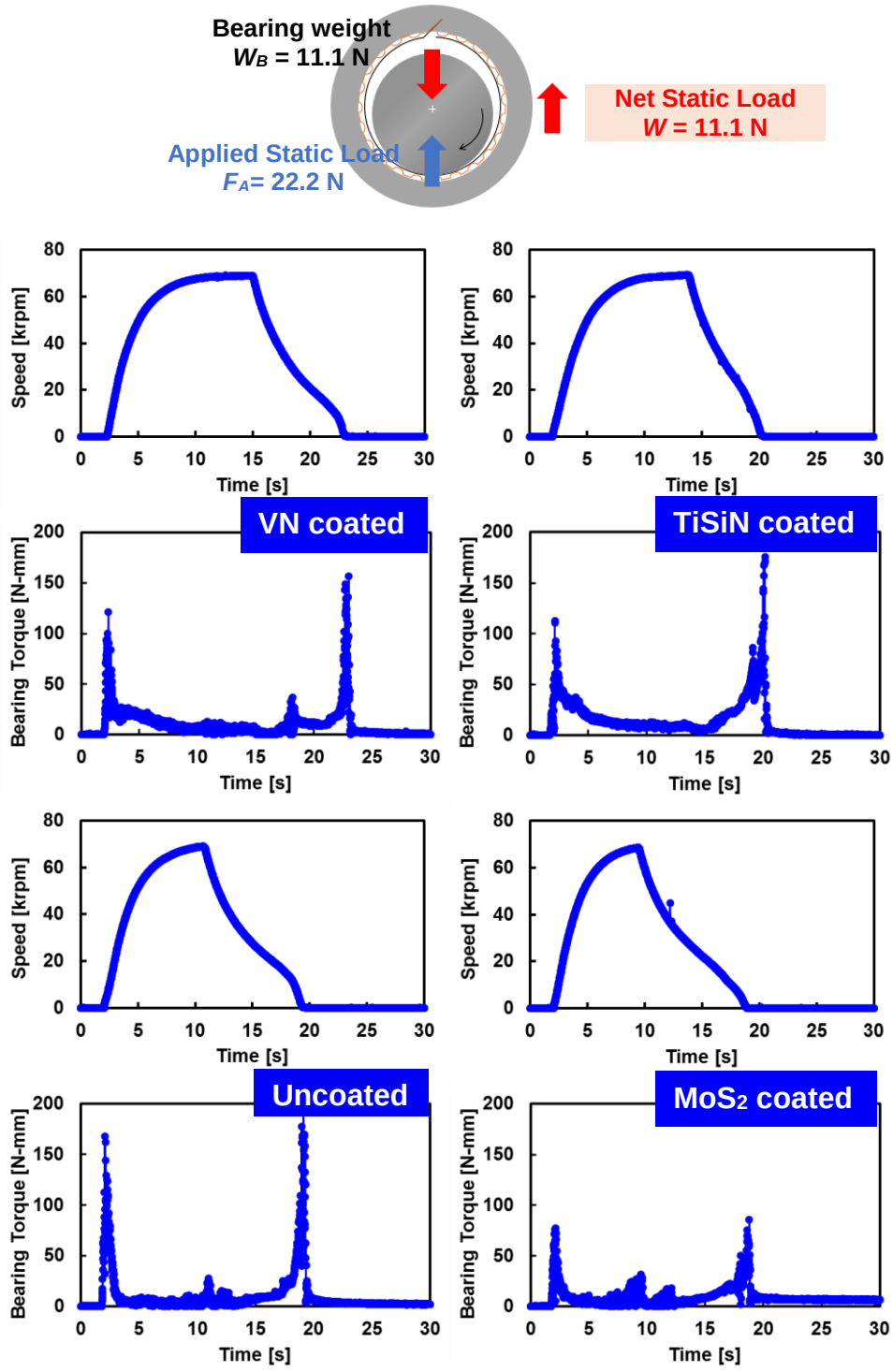

Figure 22. Recorded rotor speed and shear drag torque versus time. Four BFBs (one uncoated and three coated). Operation with net specific load *W/(LD)* = 8.0 kPa. Sample result from 10 trials.

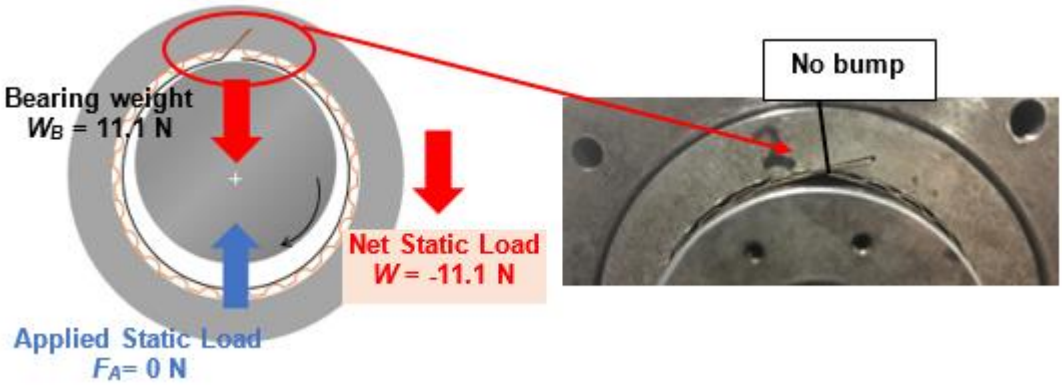

Figure 23. Detail view of fixed end of top foil in bearing. Note direction of applied load.

When the net static load W=0 N, the peak drag torque shows the lowest magnitude. In general, under a net static load of W= -11.1 N (-1 W_B, bearing weight only) the bearings offer a smaller drag torque than for operation with a net load W=11.1 N (+1 W_B). This discrepancy comes from the bearing configuration, which has a little gap (no bump) near the top foil fixed end that makes the test bearing with -1 W_B have smaller stiffness than the one with +1 W_B.

Table 5 shows the temperature rise of the test bearings and the rotor during operation. Generally, the temperature increase is too small to be significant. Recall the temperature is recorded on the bearing cartridge with a thermocouple near the inner diameter of the bearing. Note the transient start-up and shutdown process lasts a few seconds (< 20 s), hence the small increase in bearing temperature.

Table 5. Bearing cartridge temperature rise during start-up and shutdown operation. Four BFBs (one uncoated and three coated). (Uncertainty: ±0.5ºC)

Specific load [kPa] *W/(LD)*	Temperature rise [ºC] Uncoated		TiSiN		VN		MoS_2	
	Rotor	Bearing	Rotor	Bearing	Rotor	Bearing	Rotor	Bearing
-8.0	0.4	0.9	0.3	0.8	1.3	1.3	0.4	0.7
0	0.3	0.8	0.3	0.5	0.5	0.5	0.3	1.1
8.0	0.3	0.7	0.6	0.6	0.5	0.6	0.5	0.8

Figure 24 shows photographs of the top foils before and after the tests. A test called for at least 30 start-up and stop conditions. Note that all the top foils show marks of rubbing with the rotor, as displayed in Figure 25 depicting the drag torque with intermittent both small and large magnitudes near the top journal speed (70 krpm).

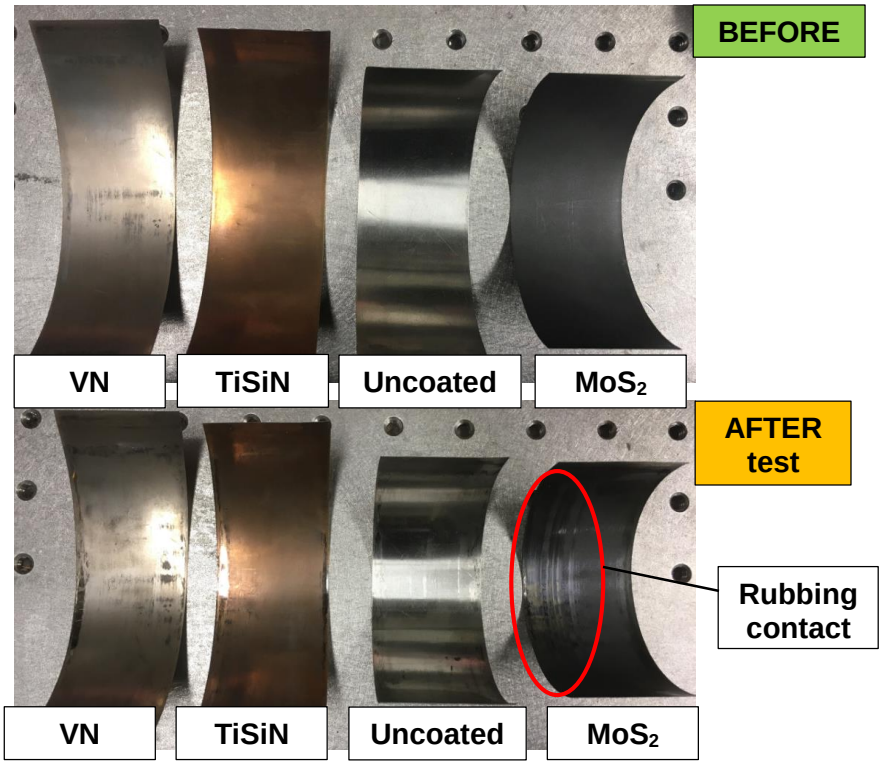

Figure 24. Photographs of top foils before and after tests (rotor start-up and shutdown processes). Four BFBs (one uncoated and three coated).

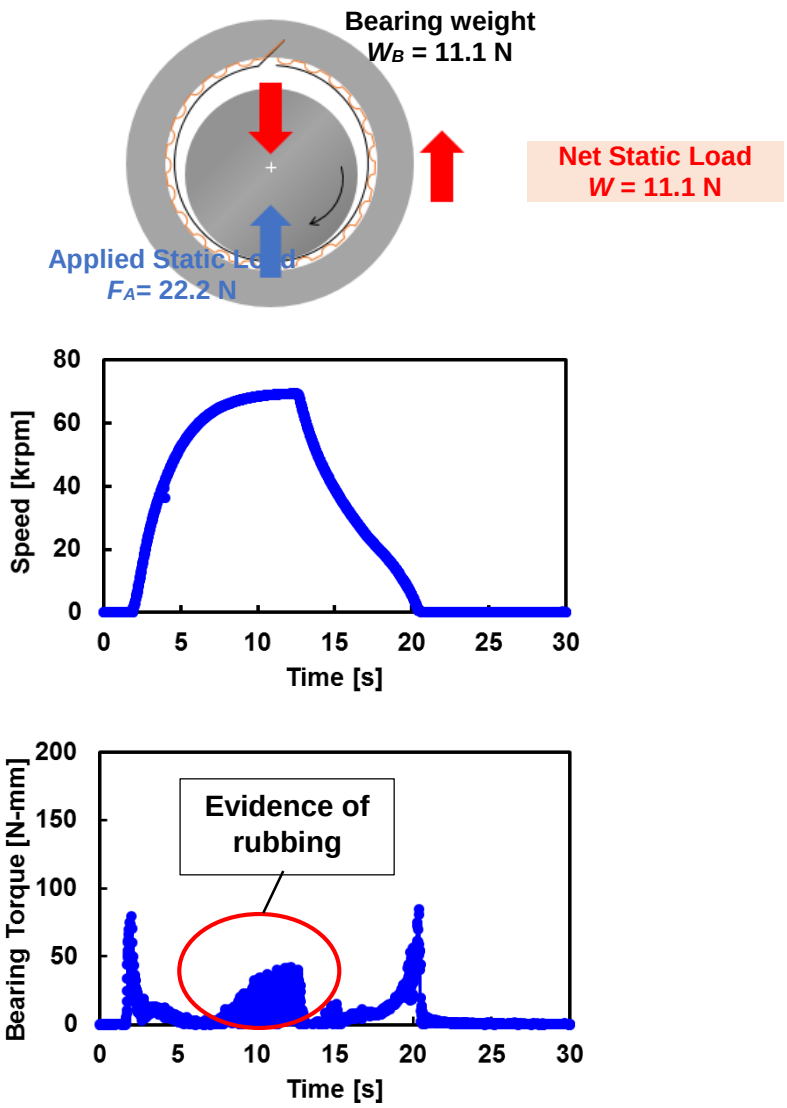

Figure 25. Recorded rotor speed and shear drag torque versus time. Operation with net specific load *W/(LD)* = 8.0 kPa. Bearing with MoS_2 coated foil.

Lift-off and touch-down rotor speeds

Figure 26 and 27 depict the rotor speed (top) and drag torque (bottom) versus time for a test BFB under a net specific load *W/(LD)*=8.0 kPa. There are two regions of large drag

torque at a low journal speed; one happens during the rotor acceleration during start up and the other during shut down as the rotor decelerates to a quick stop. These regions of high torque reveal mainly dry-sliding friction between the top foil and rotor surface. A dramatic drop in drag torque indicates the rotor lift-off to operate airborne, i.e. with a minute air film separating the rotor from the top foil.

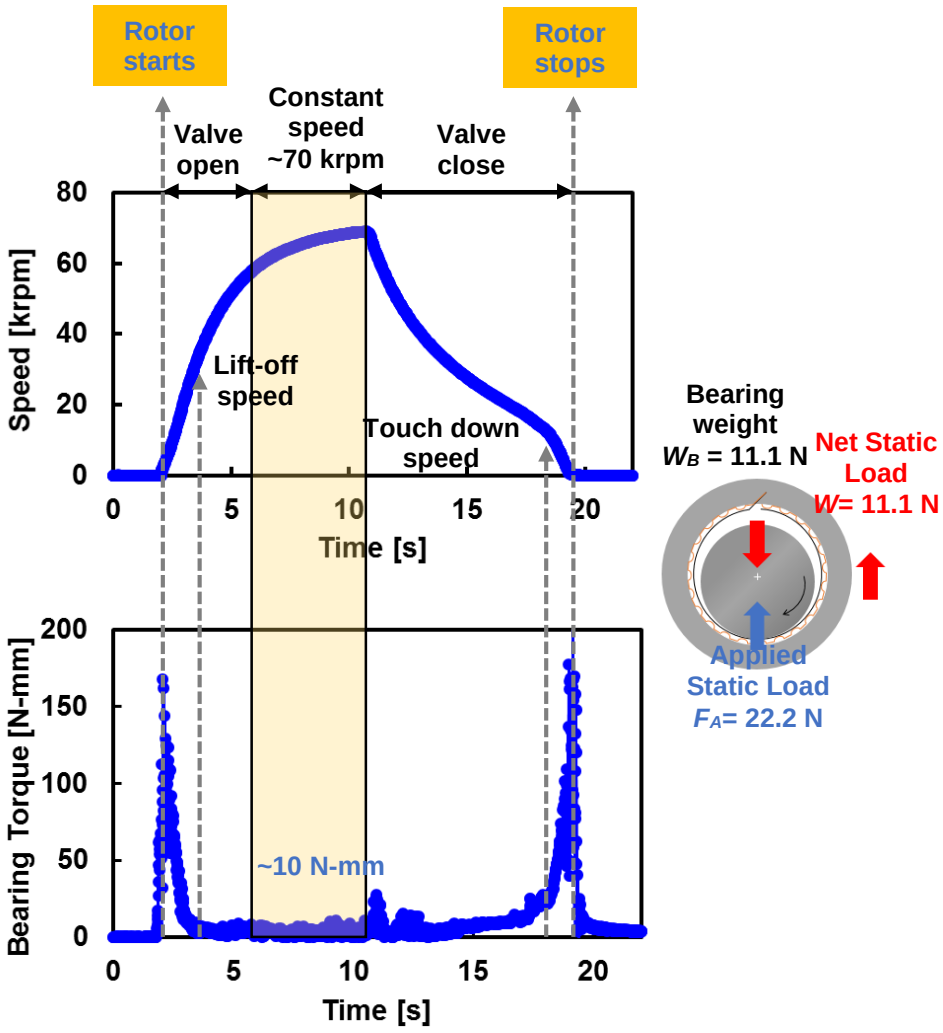

Figure 26. Test FB with uncoated top foil. Recorded rotor speed and shear drag torque versus time. Operation with net specific load *W/(LD)* = 8.0 kPa. Rotor speed-up to 70 krpm and deceleration to rest.

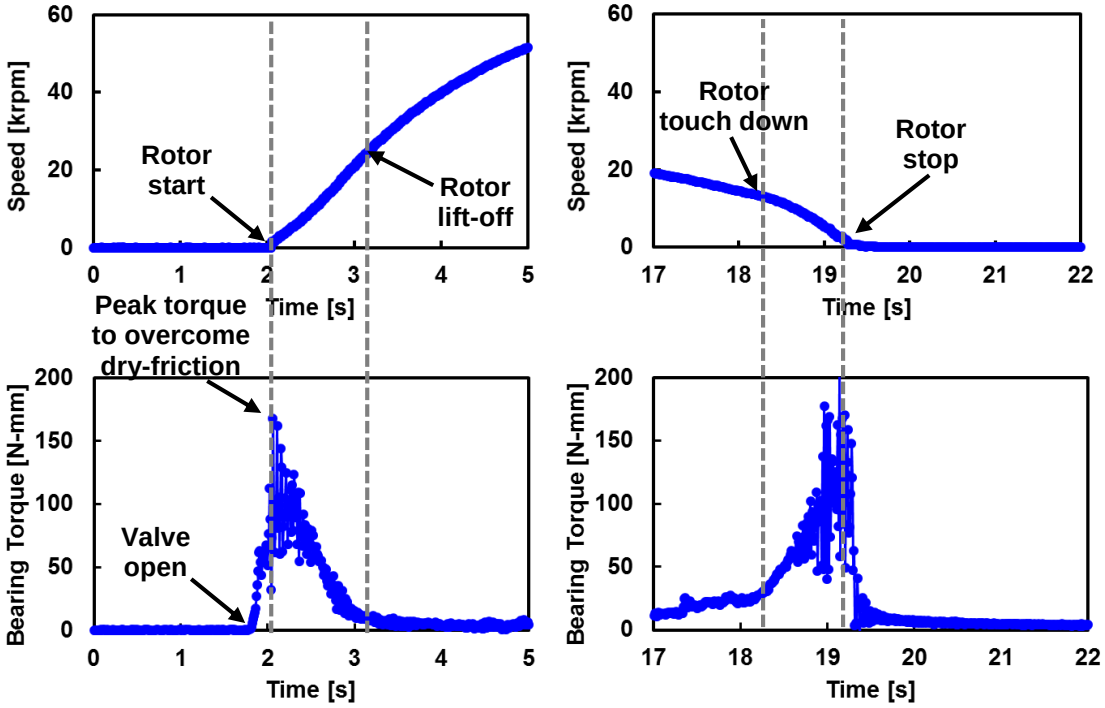

Figure 27. Test FB with uncoated top foil. Zooms of recorded rotor speed and shear drag torque versus time. Operation with net specific load *W/(LD)* = 8.0 kPa. Start-up (left) and shut-down (right) regions.

Figures 28 and 29 show the recorded drag torque for the test bearings versus rotor speed and an increasing specific load. Measurements correspond with the rotor accelerating to its top speed and decelerating to rest. The drag torque steadily decreases with rotor speed and increases with applied load. The conditions for rotor lift off and touch down are noted. The average journal lift off speed for the bearing with an uncoated top foil is higher than ~30 krpm while that of the bearing with a MoS_2 coating is lower than ~20 krpm. The journal lift-off speeds for the BFBs with either VN or a TiSiN top foil coating vary between 20~30 krpm. The average journal touch down speeds for the bearings ranges between 30 krpm to 20 krpm, except that the journal in the BFB with a TiSiN coating touches down at ~40 krpm (dry-friction sliding).

The bearing lift-off (or touch down) speed is determined as the rotor speed where the bearing drag torque ceases (or initiates) to decrease (or increase) further, thus indicating that the rotor lift-off from the bearing by an existence of a lubricating air film. Generally, once the journal is airborne, the BFB drag torque is kept consistently and small (< 10% of peak torque). However, during the tests a bearing with either VN or TiSiN coated top foil shows (at times) an unexpectedly large drag torque, likely due to intermittent contact induced by journal misalignment. Thus in these cases, the lift-off speed is determined at the instant of an abrupt change in the drag torque (> 110% of airborne torque). Appendix A shows the uncertainty in the measured drag torque is ±1 N-mm.

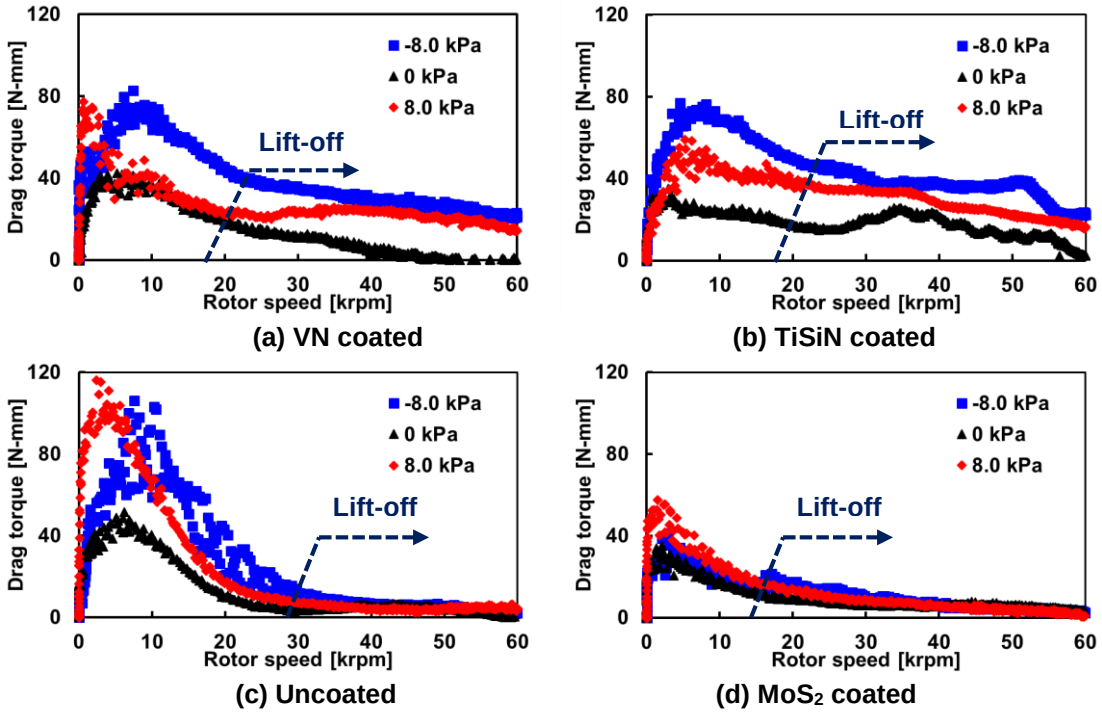

Figure 28. Recorded drag torque versus rotor speed during start-up process. Four BFBs (one uncoated and three coated). Operation with net specific load *W/(LD)* = -8.0 kPa, 0 kPa, 8.0 kPa. Average of 10 trials.

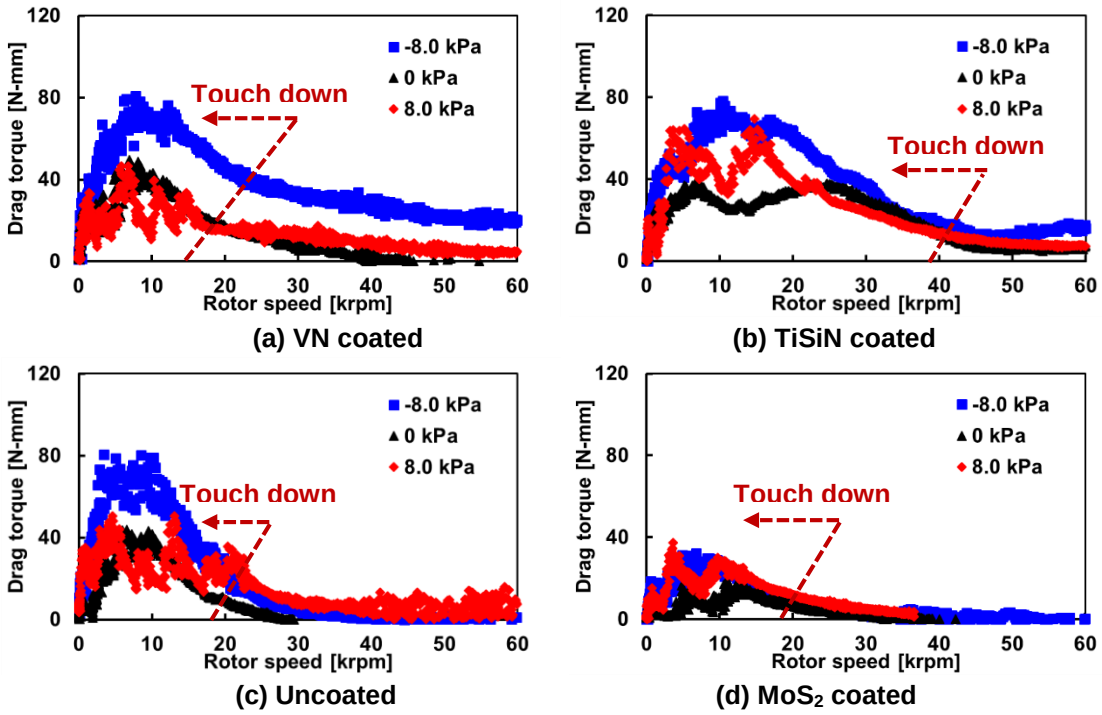

Figure 29. Recorded drag torque versus rotor speed during deceleration. Four BFBs (one uncoated and three coated). Operation with net specific load *W/(LD)* = -8.0 kPa, 0 kPa, 8.0 kPa. Average of 10 trials.

Drag friction coefficient of test bearings

The drag friction coefficient $f = T/(RW)$ is derived from the drag torque (T), the net static load (W) and the shaft radius (R). The dry-sliding friction coefficient $f_o=T_o/(RW)$ is derived[5] from the *peak* drag torque (T_o). For the four test BFBs, Figure 30 depicts f versus rotor speed during acceleration. When the rotor starts up, the dry-sliding friction coefficient f_o of the bearing with VN coating is ~0.4 while f_o for the bearing with TiSiN

[5] The dry sliding friction coefficient is identified at the instant of peak drag torque occurrence. That is, the dry-sliding friction coefficient f_o is a particular case of the drag friction f.

coating is 0.3~0.4. The uncoated bearing has the highest dry-sliding friction coefficient f_o of ~0.6, and the MoS_2 coated one has the lowest f_o of 0.2~0.3, as shown in Table 6.

Table 6. Dry-sliding friction coefficient during rotor start-up process extracted from peak drag torque. Four BFBs (one uncoated and three coated). Operation with net specific load *W/(LD)* = -8.0 kPa, 8.0 kPa. Average of 10 trials.

Specific load [kPa] *W/(LD)*	Dry-sliding friction coefficient f_o [-]			
	Uncoated	TiSiN	VN	MoS_2
-8.0	0.52	0.38	0.41	0.20
8.0	0.57	0.29	0.38	0.28

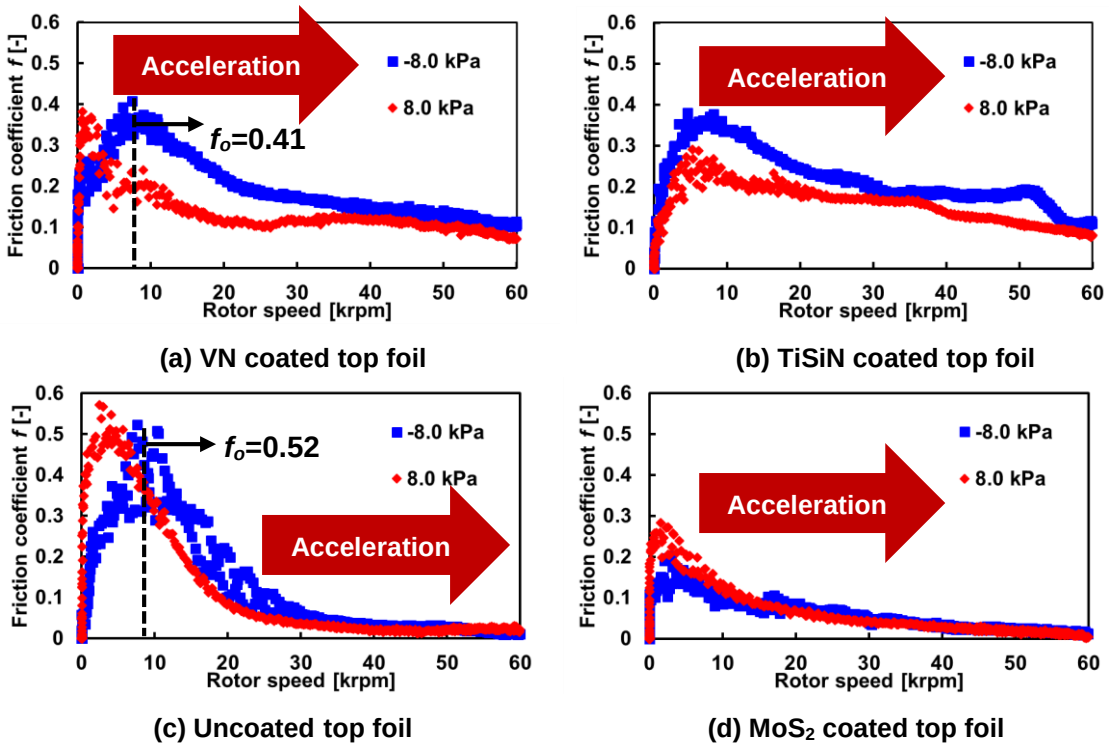

(a) VN coated top foil

(b) TiSiN coated top foil

(c) Uncoated top foil

(d) MoS_2 coated top foil

Figure 30. Drag friction coefficient versus rotor speed during rotor start-up process. Four BFBs (one uncoated and three coated).Operation with net specific load *W/(LD)* = -8.0 kPa, 8.0 kPa. Average of 10 trials.

The dry-sliding (breakaway) friction coefficient (f_o) measured during TC operation is much lower than that measured by the digital torque screwdriver under a similar applied specific load. This discrepancy likely comes from the digital torque screwdriver measuring the static friction torque at the instant the rotor turns, while only the kinetic friction torque is recorded during TC operation with missing the instant of the static friction torque occurrence because of a high initial rotational speed.

Nevertheless, both dry-sliding friction coefficients measured by TC operation and by the digital torque screwdriver show that the test bearing coated with either VN or TiSiN have a larger friction coefficient than the test top foil coated with MoS_2, thus indicating that the top foil coated with either VN or TiSiN leads to a larger energy loss than the bearing coated with MoS_2.

CHAPTER V

IDENTIFICATION OF ROTORDYNAMIC FORCE COEFFICIENTS OF THE TEST BEARINGS

Test procedure for identification of rotordynamic force coefficients

Figure 31 displays photographs of TC test rig setup for rotordynamics tests. Rotordynamic experiments are conducted to identify the force coefficients of BFBs with uncoated and coated (VN, TiSiN) Inconel top foils. In the tests, a static (vertical) load equal to 16 kPa (22.2 N) is applied. In other tests no applied static load (but the bearing assembly weight) acts on the support cage. The measurements include operation without rotor speed and with the rotor spinning at 50 krpm (833 Hz, ΩR=96 m/s).

Two orthogonally positioned electro-magnetic shakers, 45^{o} away from the direction of the static load, apply single frequency dynamic loads (F_X, F_Y) that produce bearing displacements of at most[6] 3 μm (DFT) along the axes (X,Y). The frequency range for an applied dynamic load ranges from 200 Hz to 400 Hz. The low limit (200 Hz) frequency of applied dynamic load avoids a coincidence with the structural system natural frequency (~20 Hz), and the upper limit is determined by the shaker load capacity (max. load = 100 N).

[6] Determined by the load limit of the shakers.

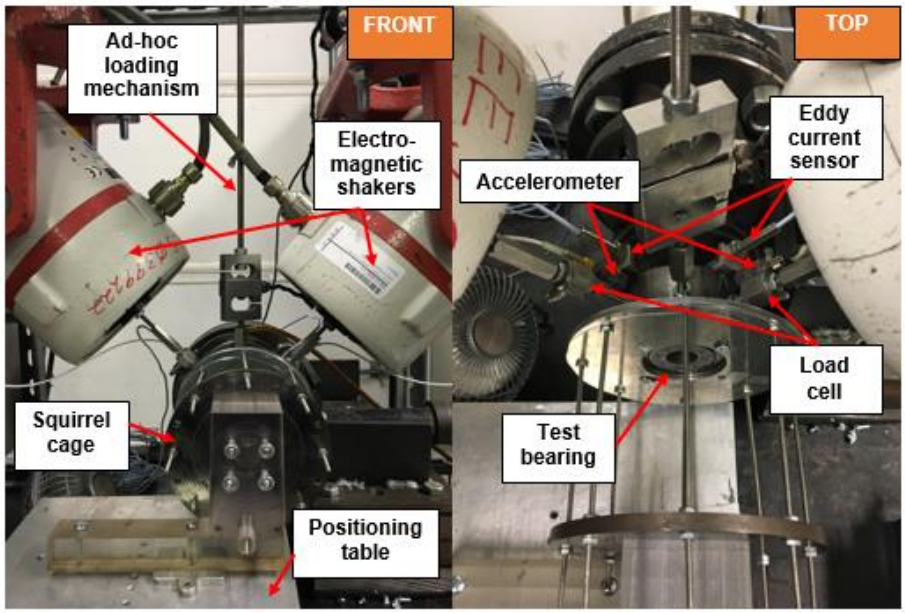

Figure 31. Photographs of TC test rig setup for rotordynamics tests.

A DAQ ad-hoc code generates a load excitation waveform lasting 1.6 s, and records 40,000 data samples of applied forces, bearing acceleration, and bearing displacement relative to the rotor. The sampling rate is 25,000 per s. A computational code processes the recorded signals and applies a Discrete Fourier analysis to extract the force coefficients according to a parameter identification procedure.

Parameter identification procedure

Figure 32 depicts a schematic view of a coordinate system for parameter identification.

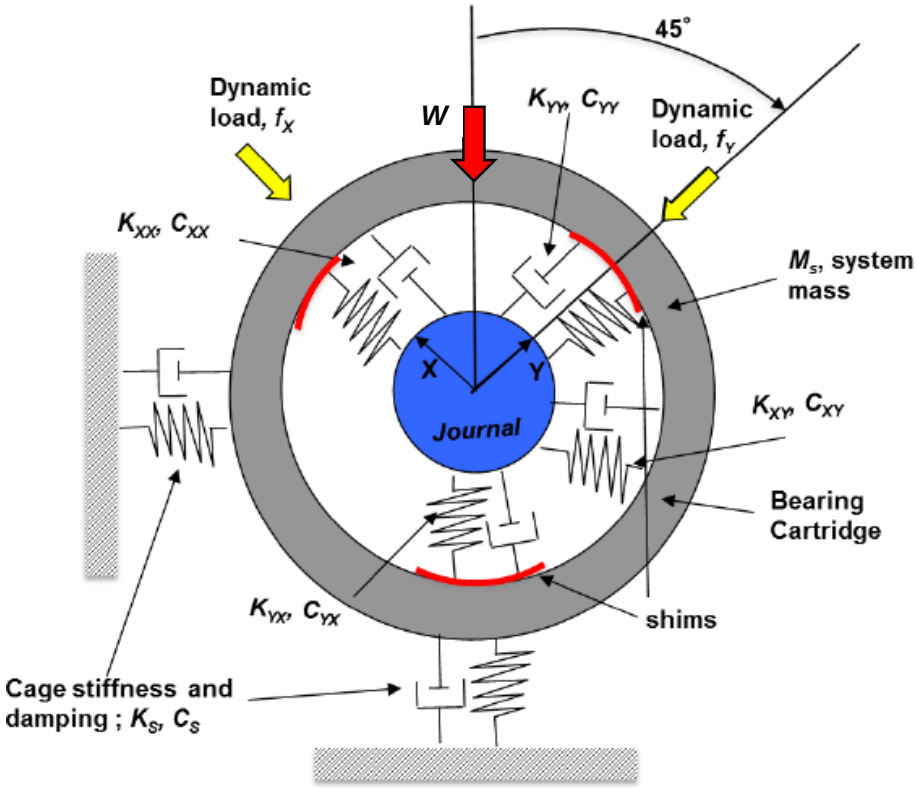

Figure 32. Schematic view of a coordinate system for a test bearing [29].

Applied dynamic forces (F_X, F_Y) excite the test bearing producing its motion. The TC journal on the flexible shaft also displaces when a dynamic load is applied to the bearing. Define (x, y) and (x_j, y_j) as the absolute bearing and journal (rotor) displacements, respectively. Hence, $(x', y') = (x, y) - (x_j, y_j)$ are the bearing displacements relative to the journal.

The equation of motion for the test bearing is

$$\begin{bmatrix} M_{S_X} & 0 \\ 0 & M_{S_Y} \end{bmatrix} \begin{Bmatrix} \ddot{x} \\ \ddot{y} \end{Bmatrix} + \begin{bmatrix} C_{S_X} & 0 \\ 0 & C_{S_Y} \end{bmatrix} \begin{Bmatrix} \dot{x} \\ \dot{y} \end{Bmatrix} + \begin{bmatrix} K_{S_X} & 0 \\ 0 & K_{S_Y} \end{bmatrix} \begin{Bmatrix} x \\ y \end{Bmatrix} + \begin{bmatrix} C_{XX} & C_{XY} \\ C_{YX} & C_{YY} \end{bmatrix} \begin{Bmatrix} \dot{x}' \\ \dot{y}' \end{Bmatrix} + \begin{bmatrix} K_{XX} & K_{XY} \\ K_{YX} & K_{YY} \end{bmatrix} \begin{Bmatrix} x' \\ y' \end{Bmatrix} = \begin{Bmatrix} F_X \\ F_Y \end{Bmatrix} \tag{1}$$

where $(K_{\alpha\beta}, C_{\alpha\beta})_{\alpha\beta=X,Y}$ are BFB frequency dependent stiffness and damping coefficients. The effective system mass $(M_S)_{X,Y}$, cage stiffness $(K_S)_{X,Y}$ and cage damping coefficients $(C_S)_{X,Y}$ are estimated from impact loads prior to the experiments. See Appendix B for complete details on the estimation of the structural parameters. Note Eq. (1) omits any force arising from journal imbalance or any other source.

The time domain excitation forces and resulting BFB motions are transformed into the frequency domain by applying the Discrete Fourier Transform (DFT), i.e.,

$$\overline{F}_{X(\omega)} = DFT\left(F_{X(t)}\right) \; ; \; \overline{x'}_{(\omega)} = DFT\left(x'_{(t)}\right) \; ; \; \overline{A}_{X(\omega)} = DFT(\ddot{x}_{(t)}) \tag{2}$$

and likewise for displacements and other variables along the *Y* direction. Recall that also

$$DFT[\dot{x}'_{(t)}] = j\omega \overline{x'}_{(\omega)}, \; DFT[\dot{x}_{(t)}] = \frac{\overline{A}_{X(\omega)}}{j\omega}, \; DFT[x_{(t)}] = -\frac{\overline{A}_{X(\omega)}}{\omega^2} \tag{3}$$

where $j = \sqrt{-1}$.

The equation of motion in the frequency domain becomes algebraic and written as

$$\begin{bmatrix} K_{XX} + j\omega C_{XX} & K_{XY} + j\omega C_{XY} \\ K_{YX} + j\omega C_{YX} & K_{YY} + j\omega C_{YY} \end{bmatrix} \begin{bmatrix} \overline{x}'_{(\omega)} \\ \overline{y}'_{(\omega)} \end{bmatrix} = \begin{bmatrix} \overline{G}_{X(\omega)} \\ \overline{G}_{Y(\omega)} \end{bmatrix} = \begin{bmatrix} \overline{F}_{X(\omega)} \\ \overline{F}_{Y(\omega)} \end{bmatrix} - \begin{bmatrix} M_{S_X} + \dfrac{C_{S_X}}{j\omega} - \dfrac{K_{S_X}}{\omega^2} \\ M_{S_Y} + \dfrac{C_{S_Y}}{j\omega} - \dfrac{K_{S_Y}}{\omega^2} \end{bmatrix} \begin{bmatrix} \overline{A}_{X(\omega)} \\ \overline{A}_{Y(\omega)} \end{bmatrix} \tag{4}$$

where ($\bar{x}'_{(\omega)}$,$\bar{y}'_{(\omega)}$) are the DFTs of the bearing relative displacements, ($\bar{F}_{X(\omega)}$,$\bar{F}_{Y(\omega)}$) are the DFTs of the excitation forces, and ($\bar{A}_{X(\omega)}$,$\bar{A}_{Y(\omega)}$) are the DFTs of the bearing accelerations.

The condensed form of the equation of motion in the frequency domain equation is

$$\begin{bmatrix} H_{XX} & H_{XY} \\ H_{YX} & H_{YY} \end{bmatrix} \begin{bmatrix} \bar{x}'_{(\omega)} \\ \bar{y}'_{(\omega)} \end{bmatrix} = \begin{bmatrix} \bar{G}_{X(\omega)} \\ \bar{G}_{Y(\omega)} \end{bmatrix} \tag{5}$$

where $\mathbf{H}_{(\omega_k)}=(\mathbf{K}+j\omega_k\mathbf{C})$ is the matrix of bearing complex stiffness coefficients at the excitation frequency (ω_k).

Two independent load excitations are required to determine the eight components of the complex stiffness **H.** The applied loads are $\mathbf{F}^{\mathrm{X}}=[F_X\ 0]^{\mathrm{T}}$, and $\mathbf{F}^{\mathrm{Y}}=[F_Y\ 0]^{\mathrm{T}}$, respectively. The equations for the two sets of dynamic load vectors become

$$\begin{bmatrix} H_{XX} & H_{XY} \\ H_{YX} & H_{YY} \end{bmatrix} \begin{bmatrix} \bar{x}^{X}_{(\omega)} & \bar{x}^{Y}_{(\omega)} \\ \bar{y}^{X}_{(\omega)} & \bar{y}^{Y}_{(\omega)} \end{bmatrix} = \begin{bmatrix} \bar{G}^{X}_{X(\omega)} & \bar{G}^{Y}_{X(\omega)} \\ \bar{G}^{X}_{Y(\omega)} & \bar{G}^{Y}_{Y(\omega)} \end{bmatrix} \tag{6}$$

$$\mathbf{H}\bar{\mathbf{z}}=\bar{\mathbf{G}} \tag{7}$$

The first column in the $\bar{z}$ matrix contains the bearing displacements (relative to the journal) along the *X* and *Y* axis due to applied dynamic load along the *X* axis ($\mathbf{F}^{\mathrm{X}}$), while the second column denotes the bearing relative displacements due to ($\mathbf{F}^{\mathrm{Y}}$). At each frequency (ω_k), the bearing complex stiffness coefficients are

$$\mathbf{K}_{(\omega_k)}+j\omega_k\mathbf{C}_{(\omega_k)}=\mathbf{H}_{(\omega_k)}=\bar{\mathbf{G}}_{(\omega_k)}\bar{\mathbf{z}}^{-1}_{(\omega_k)} \tag{8}$$

Thus, $$\{K_{\alpha\beta}\}_{(\omega_k)} \leftarrow \mathrm{Re}\left(\{H_{\alpha\beta}\}_{\omega_k}\right),\ \{C_{(\omega_k)}\}_{\alpha\beta} \leftarrow \frac{\mathrm{Im}(\{H_{\alpha\beta}\}_{\omega_k})}{j\omega_k},\ \alpha\beta=X,Y \tag{9}$$

Data analysis

Note that more mechanical energy is required to produce the same displacement amplitudes at high frequencies, thus the dynamic load is controlled (amplitude typically increases with excitation frequency) to maintain a constant bearing displacement amplitude (relative to the journal) across the excitation frequency range.

For operation with journal speed (airborne and with a full film), the force coefficients of the gas film act in series with the bump foil under-spring structure. During the tests, the temperature of the bearing cartridge and shaft rose ~30°C, as in Figure 33. Once the gas film forms, separating the shaft from the top foil, the bearing cartridge and test shaft temperature stabilize at ~51°C (30°C above ambient) and cease to increase further.

Figure 33. Photographs of bearing cartridge and shaft – measurement of temperature. (left : 0 krpm, ~20.6 ºC, right : at 50 krpm, ~50.7 ºC)

Note that as the temperature of the gas lubricant increases so does its viscosity. Further, the test shaft experiences thermal and centrifugal growth which act to decrease the bearing

clearance, thereby affecting the bearing force coefficients. A BFB stiffness will decrease with a large rise in the bearing temperature due to a reduction in the elastic modulus of the bump foil and top foil strips. Presently, this effect is likely minimal.

The dynamic loads applied are single-frequency (periodic). The frequency ranges from 200 Hz to 400 Hz in steps of 20 Hz.

A coordinate transformation[7] is used to determine the force coefficients with respect to a coordinate system ($\underline{X}$, $\underline{Y}$) where $\underline{X}$ is parallel to the vertical plane (the applied load direction) and $\underline{Y}$ is horizontal. The transformation allows to compare the results with the earlier measurements in Ref. [29].

$$\begin{bmatrix} \underline{K_{XX}} & \underline{K_{XY}} \\ \underline{K_{YX}} & \underline{K_{YY}} \end{bmatrix} \tag{10}$$

$$= \begin{bmatrix} K_{XX}cos^2(\varphi)+K_{YY}sin^2(\varphi) & K_{XX}\,cos(\varphi)\,sin(\varphi) - K_{YY}cos(\varphi)sin(\varphi) \\ K_{XX}\,cos(\varphi)\,sin(\varphi) - K_{YY}cos(\varphi)sin(\varphi) & K_{YY}cos^2(\varphi)+K_{XX}sin^2(\varphi) \end{bmatrix}$$

Hence,

$$\begin{aligned} \underline{K_{XX}}=\underline{K_{YY}}&=\frac{1}{2}(K_{XX}+K_{YY}) \\ \underline{K_{XY}}=\underline{K_{YX}}&=\frac{1}{2}(K_{XX}-K_{YY}) \end{aligned} \tag{11}$$

where $\varphi=\pi/4$, and ideal for $\underline{C_{XX}}=\underline{C_{YY}}$, $\underline{C_{XY}}=\underline{C_{YX}}$.

[7] The transformed complex stiffness matrix $\underline{H}$ for the $\underline{X,Y}$ coordinate system takes the form $\mathbf{\underline{H}}=\mathbf{PHP}^{\mathrm{T}}$, where the coordinate transformation matrix $\mathbf{P}=\begin{bmatrix} cos(\varphi) & sin(\varphi) \\ -sin(\varphi) & cos(\varphi) \end{bmatrix}$, where φ is the angle from the $\underline{Y}$ axis to the Y axis.

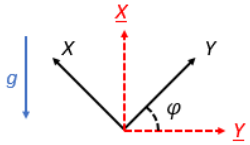

Dynamic force coefficients for the test bearings

Figures 34 and 35 show the stiffness ($\underline{K_{XX}}=\underline{K_{YY}}$, $\underline{K_{XY}}=\underline{K_{YX}}$) coefficients versus excitation frequency for the test uncoated-BFB for operation without journal rotation and with journal rotation at ~50 krpm (833 Hz), and without a static load and with a static (vertical upwards) load of 16 kPa. The maximum uncertainty in the stiffness coefficients is ±0.08 MN/m, and the maximum variability is 0.05 MN/m (see Appendix A). Hence the total uncertainty is 0.13 MN/m.

The BFB cross coupled stiffness coefficients ($\underline{K_{XY}}=\underline{K_{YX}}$) are small (less than ~10% of the maximum direct stiffness). The direct stiffness coefficients ($\underline{K_{XX}}=\underline{K_{YY}}$) increase with excitation frequency, being larger for the 16 kPa load condition than without an applied load, as expected. The BFB $\underline{K_{XX}}=\underline{K_{YY}}$ with journal rotation of 50 krpm (833 Hz) are smaller than those without journal rotation, which means the presence of a gas film acting in series with the under-spring structure reduces the BFB stiffnesses.

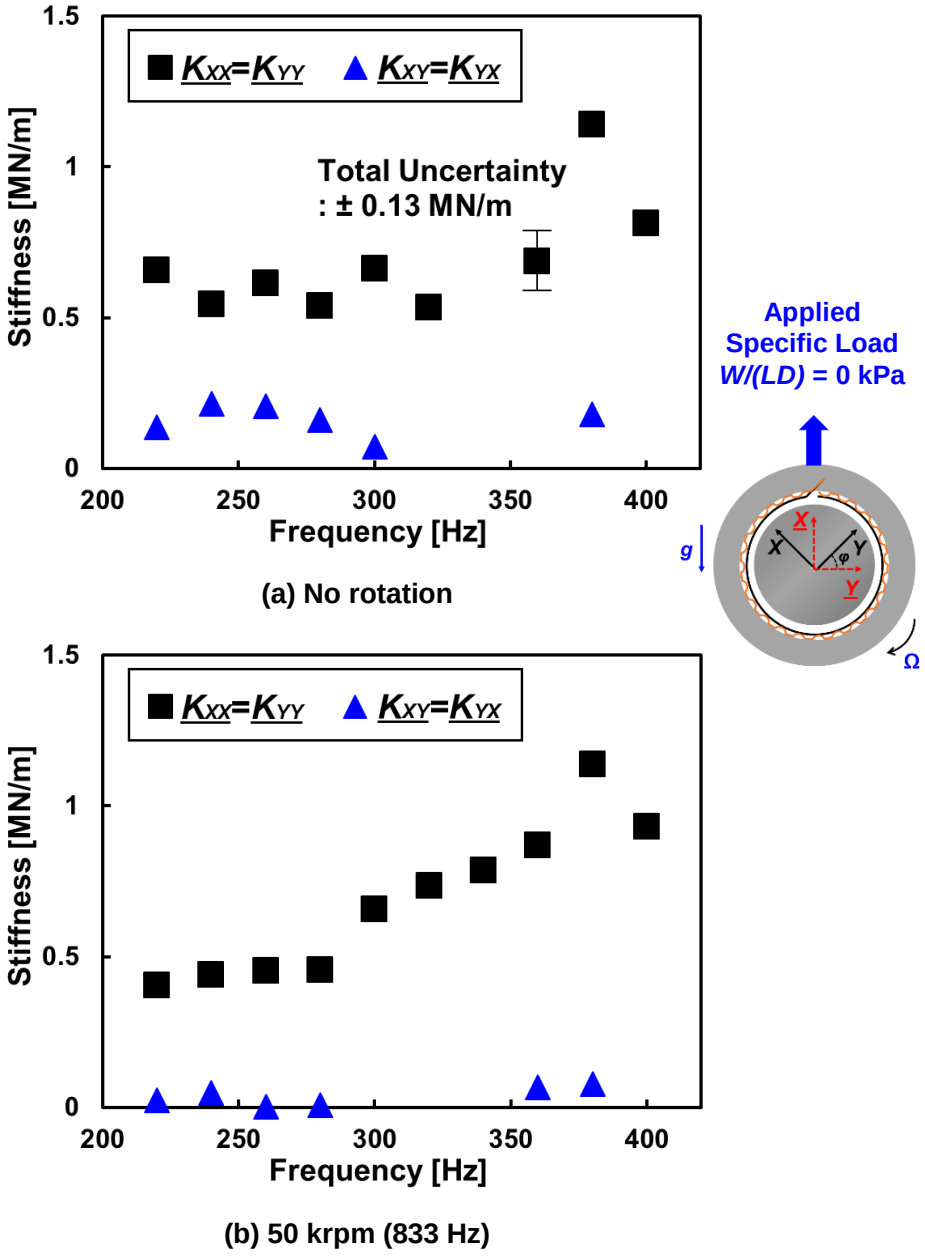

Figure 34. Stiffness coefficients (K_{XX}=K_{YY}, K_{XY}=K_{YX}) versus excitation frequency for test BFB with uncoated top foil. Operation without and with rotor speed at 50 krpm (833Hz), and without static load. Dynamic single frequency loads from 200-400 Hz. Average 10 excitations.

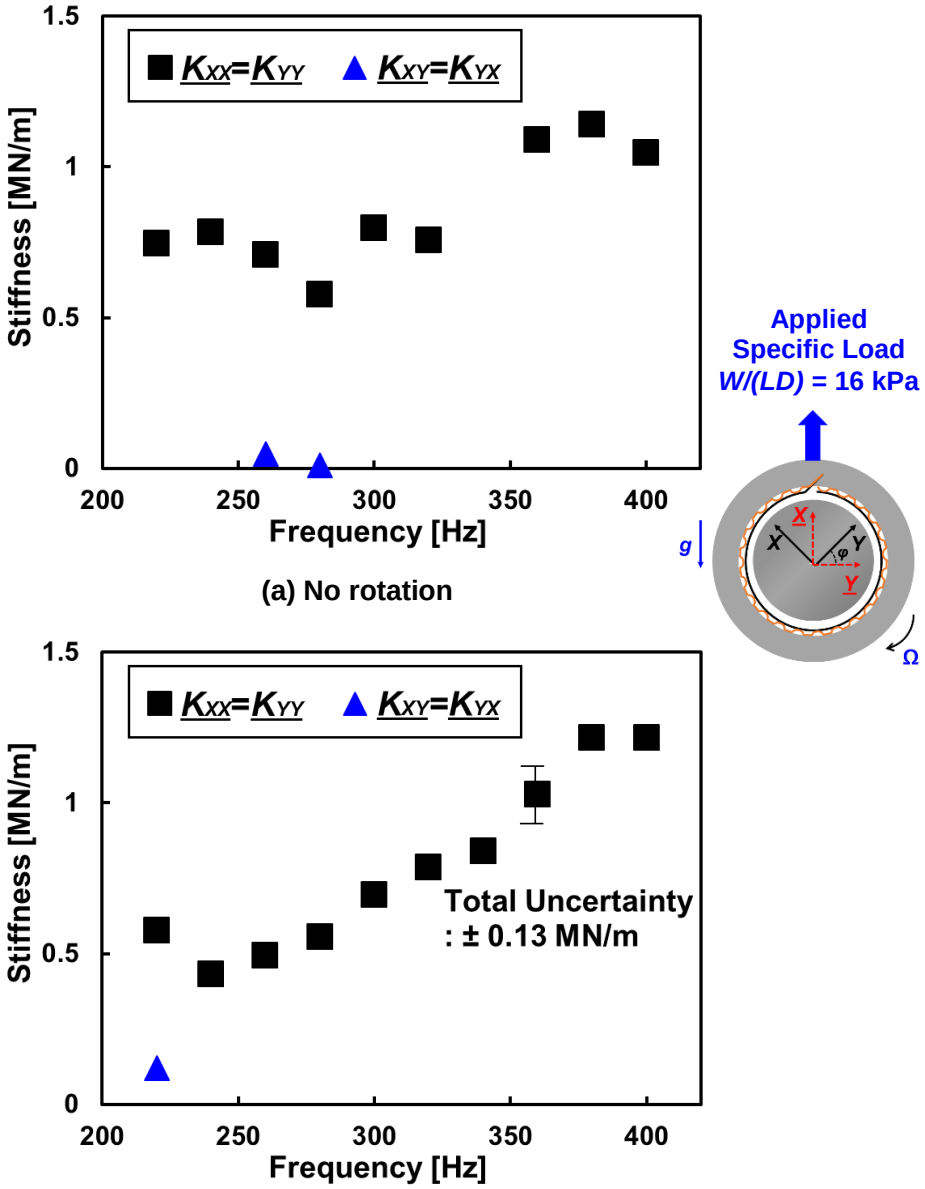

Figure 35. Stiffness coefficients ($K_{XX}=K_{YY}$, $K_{XY}=K_{YX}$) versus excitation frequency for test BFB with uncoated top foil. Operation without and with rotor speed at 50 krpm (833Hz), and under a static load of 16 kPa. Dynamic single frequency loads from 200-400 Hz. Average 10 excitations.

The test results reveal one third lower direct stiffnesses when compared to earlier measurements in Ref. [29]. Norsworthy reports $\underline{K_{XX}}$ and $\underline{K_{YY}}$ are ~1 MN/m at 250 Hz and eventually growing up to ~2.5 MN/m at 450 Hz for both stationary and rotation of 50 krpm (833 Hz) under a 14.3 kPa static load, as shown in Figure 36. The direct stiffnesses for both the current and prior tests increase with an increase in excitation frequency. The prior tests [29] give larger magnitudes of direct stiffness. The discrepancy comes from differences of the under-spring structure (bump layer strips geometry).

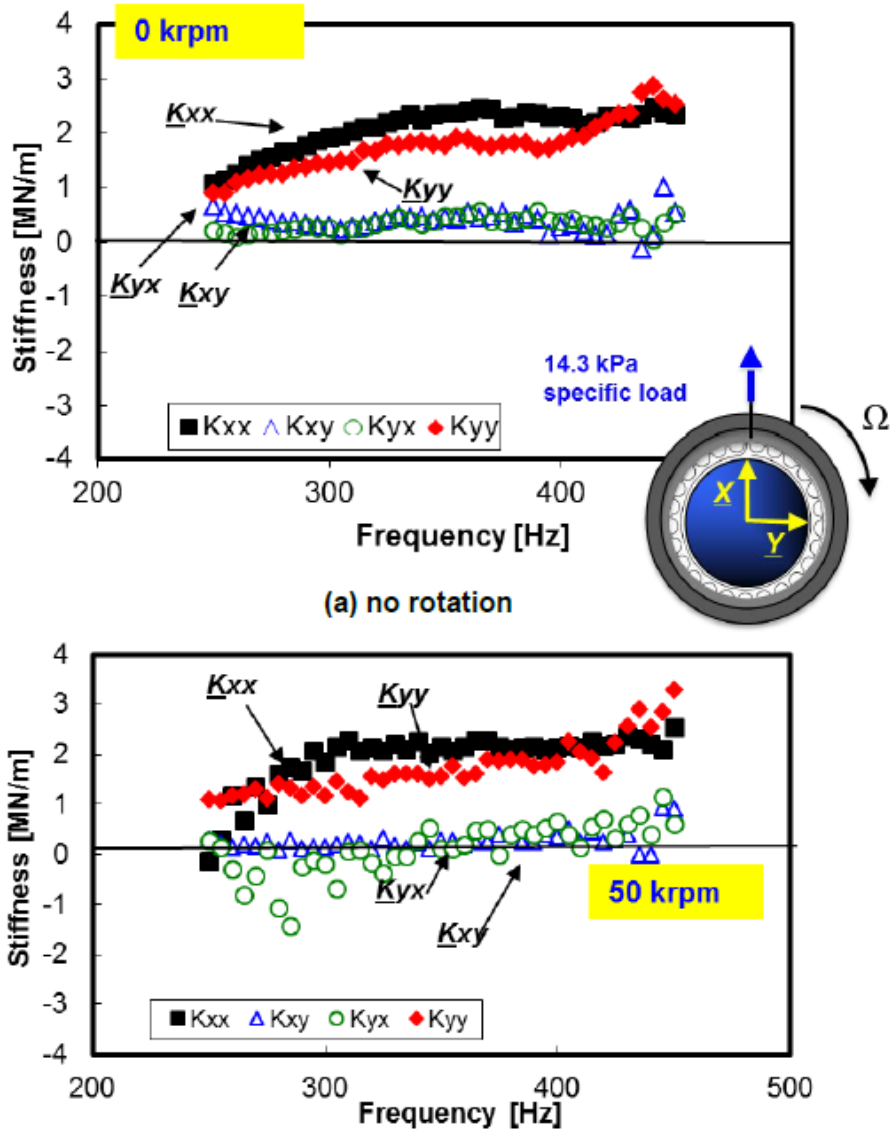

Figure 36. Stiffness coefficients ($\underline{K}_{XX}$, $\underline{K}_{YY}$, $\underline{K}_{XY}$, $\underline{K}_{YX}$) versus excitation frequency for test BFB with uncoated top foil taken from Ref. [29]. Operation without and with rotor speed at 50 krpm (833Hz), and under a static load of 14.3 kPa. Dynamic sine sweep loads from 250-450 Hz. Average 10 excitations.

Figure 37 and 38 show the damping coefficients ($\underline{C_{XX}}=\underline{C_{YY}}$, $\underline{C_{XY}}=\underline{C_{YX}}$) versus excitation frequency for the test uncoated-BFB for operation without journal rotation and with journal rotation at ~50 krpm (833 Hz), and without a static load and with a static (vertical upwards) load of 16 kPa. The maximum uncertainty in the damping coefficients is ±80 Ns/m, and the maximum variability is 30 Ns/m (see Appendix A).

The direct damping coefficients ($\underline{C_{XX}}=\underline{C_{YY}}$) are larger under an applied specific load of 16 kPa than those without a static load. $\underline{C_{XX}}=\underline{C_{YY}}$ with journal rotation at 50 krpm (833 Hz) has lower magnitude than those coefficients without journal rotation. This is because the gas film acts in a series with its under-spring structure. The cross coupled damping coefficients ($\underline{C_{XY}}=\underline{C_{YX}}$) are much lower than the direct ones. The damping coefficients decrease steadily with excitation frequency.

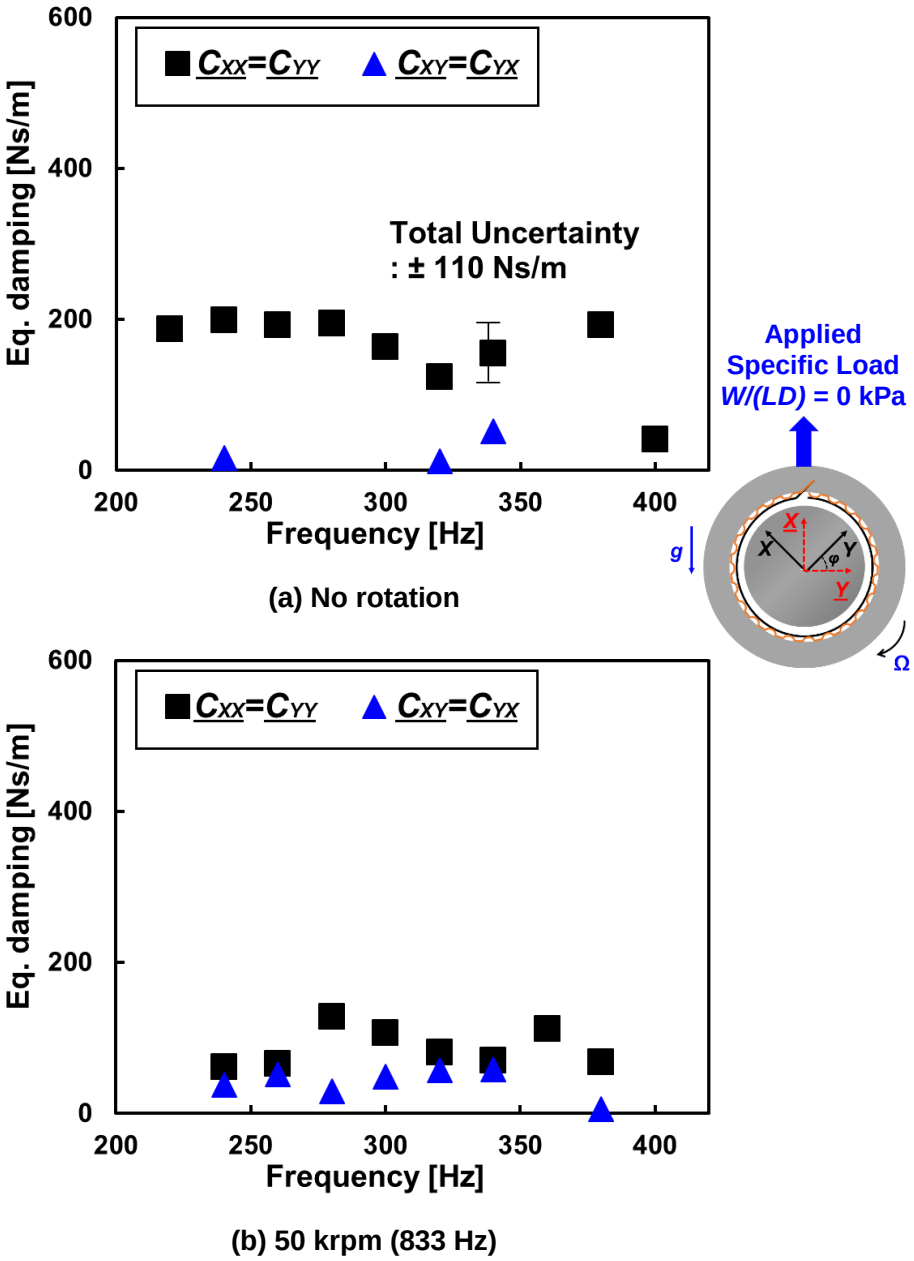

Figure 37. Damping coefficients (C_{XX}=C_{YY}, C_{XY}=C_{YX}) versus excitation frequency for test BFB with uncoated top foil. Operation without and with rotor speed at 50 krpm (833Hz), and without static load. Dynamic single frequency loads from 200-400 Hz. Average 10 excitations.

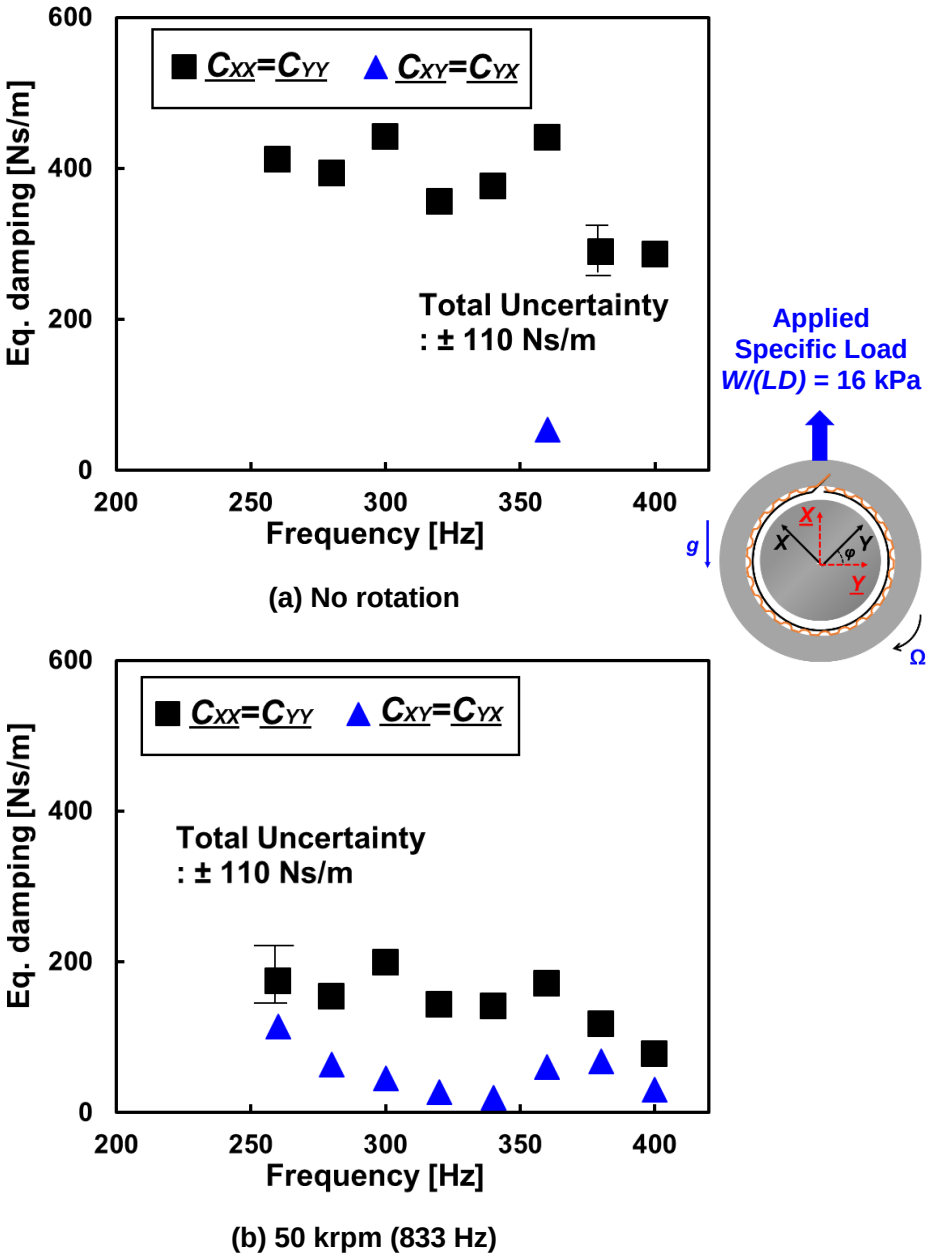

Figure 38. Damping coefficients (C_{XX}=C_{YY}, C_{XY}=C_{YX}) versus excitation frequency for test BFB with uncoated top foil. Operation without and with rotor speed at 50 krpm (833Hz), and under a static load of 16 kPa. Dynamic single frequency loads from 200-400 Hz. Average 10 excitations.

Figure 39 shows earlier of damping coefficients ($\underline{C_{XX}}$, $\underline{C_{YY}}$, $\underline{C_{XY}}$, $\underline{C_{YX}}$) [29] versus excitation frequency for a test BFB with an uncoated top foil operating under a static load of 14.3 kPa. The excitation is a dynamic sine sweep load, 250-450 Hz. The direct damping coefficients for both measurements (current and prior) decrease with an increase in excitation frequency, while the magnitude of the prior results shows twice as much damping. This discrepancy comes from difference of the structural damping for the test bearings since they have different under-spring structure (bump layer strips geometry).

Figure 40 and 41 show a comparison of the stiffness and damping coefficients for the test BFB uncoated and coated with VN and TiSiN operating with journal speed at 50 krpm (833 Hz) under static load of 16 kPa. The BFB direct stiffness coefficients ($\underline{K_{XX}}$=$\underline{K_{YY}}$) increase (0.5~1.0 MN/m) with an increase in excitation frequency, whereas the BFB direct damping coefficients ($\underline{C_{XX}}$=$\underline{C_{YY}}$) decrease. Note that the stiffnesses are largely determined by the under spring structure, while the BFB damping coefficients are largely affected by the dry-sliding friction coefficient (Coulomb friction) of the coating on the back surface of top foil.

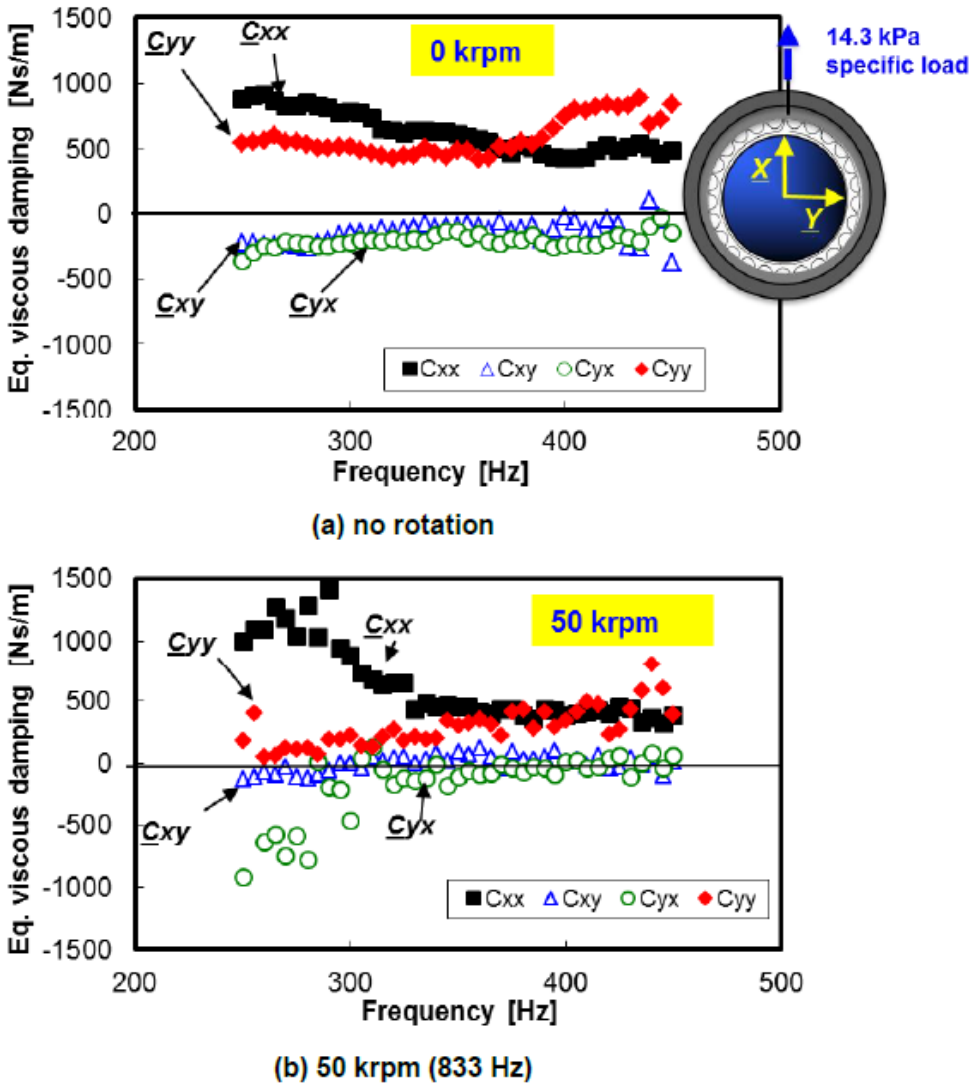

Figure 39. Damping coefficients (C_{XX}, C_{YY}, C_{XY}, C_{YX}) versus excitation frequency for test BFB with uncoated top foil taken from Ref. [29]. Operation without and with rotor speed at 50 krpm (833Hz), and under a static load of 14.3 kPa. Dynamic sine sweep loads from 250-450 Hz. Average 10 excitations.

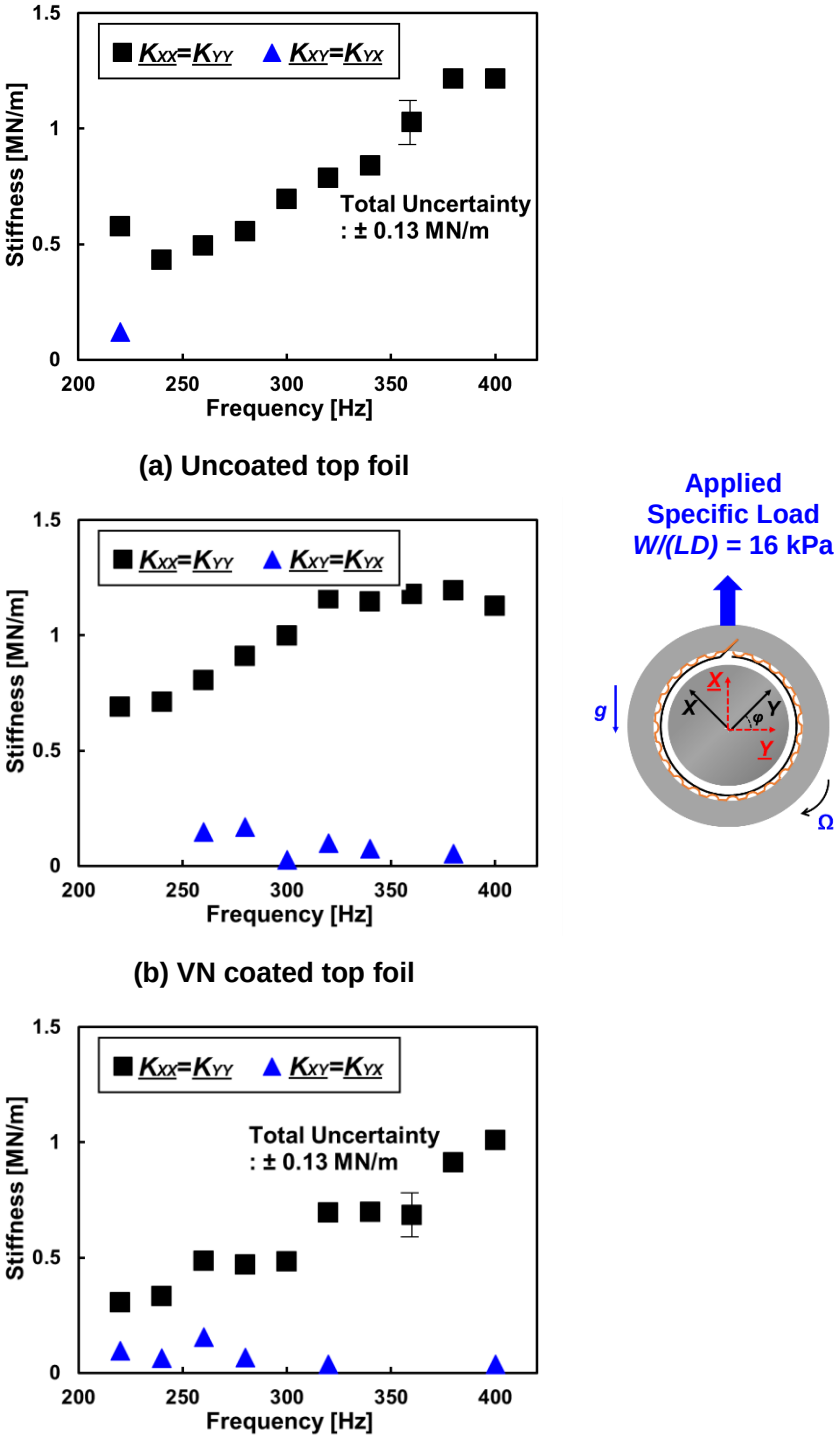

Figure 40. Stiffness coefficients (K_{XX}=K_{YY}, K_{XY}=K_{YX}) versus excitation frequency for test BFBs. Journal rotation of 50 krpm (833 Hz) and with static load of 16 kPa.
Dynamic single frequency loads from 200-400 Hz. Average 10 excitations.

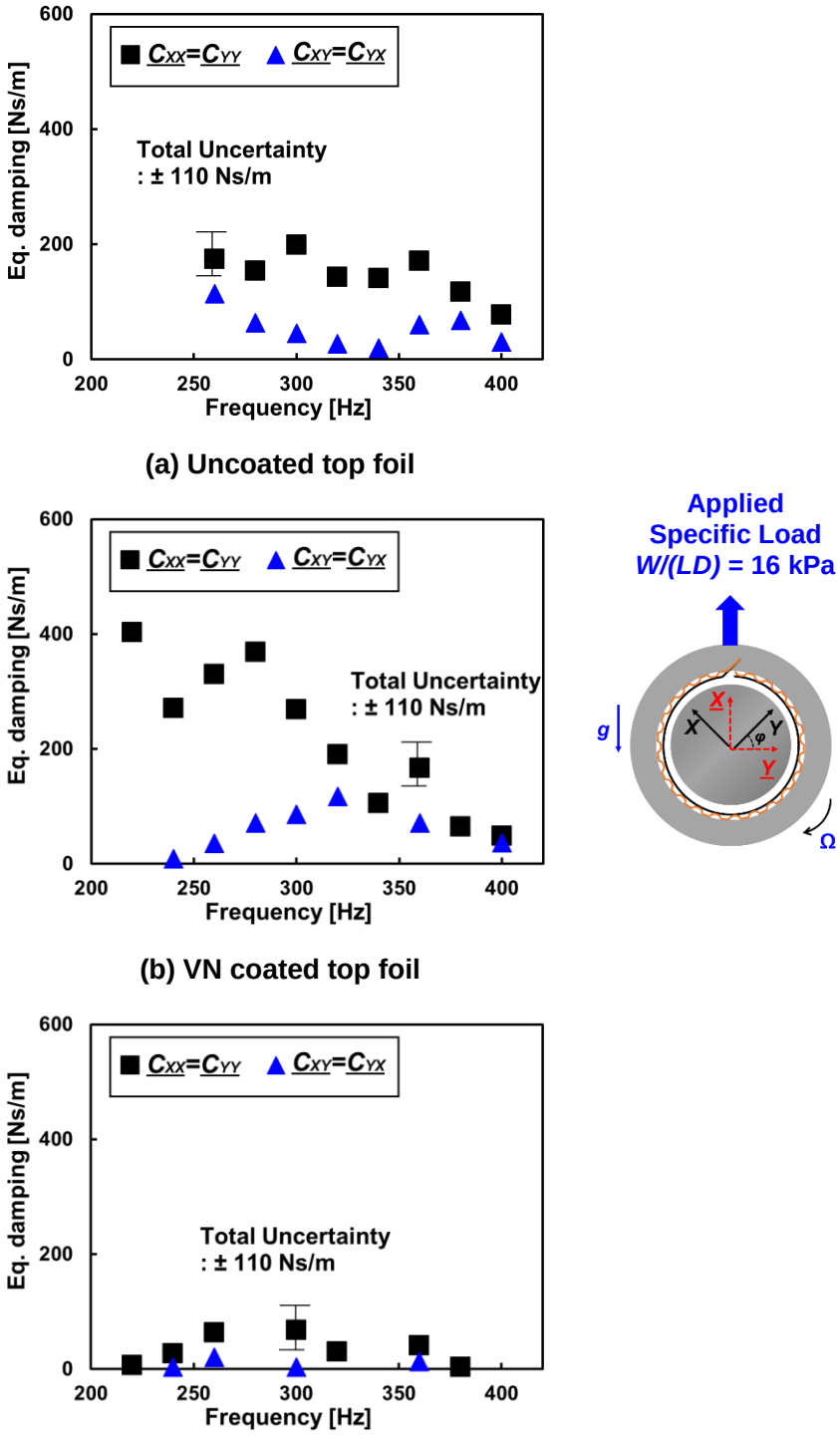

Figure 41. Damping coefficients (C_{XX}=C_{YY}, C_{XY}=C_{YX}) versus excitation frequency for test BFBs. Journal rotation of 50 krpm (833 Hz) and with static load of 16 kPa.
Dynamic single frequency loads from 200-400 Hz. Average 10 excitations.

Foil bearing material loss factor

Figure 42 presents the loss factor (γ) versus excitation frequency for the test top foils (one uncoated and three coated) operating with journal speed at 50 krpm (833 Hz) under a static load of 16 kPa. The material loss factor

$$\gamma=\omega(C_{XX}+C_{YY})/(K_{XX}+K_{YY}) \quad (12)$$

γ is a measure of mechanical energy dissipation. γ decreases rapidly with an increase in excitation frequency. At a frequency below 300 Hz, a too large γ is removed due to the smallness of the stiffness coefficients. The variation in the loss factor with varying excitation frequency is due to the force coefficients which also vary with frequency.

The loss factor of the BFB coated with VN shows comparable magnitude with that of the uncoated BFB, while indicating that the VN coated top foil dissipates more mechanical energy during full film operation than the top foil coated with TiSiN. Note that the loss factor of the TiSiN coated top foil shows $\gamma \rightarrow 0$ since the stiffnesses increase with excitation frequency whereas the damping coefficients decrease.

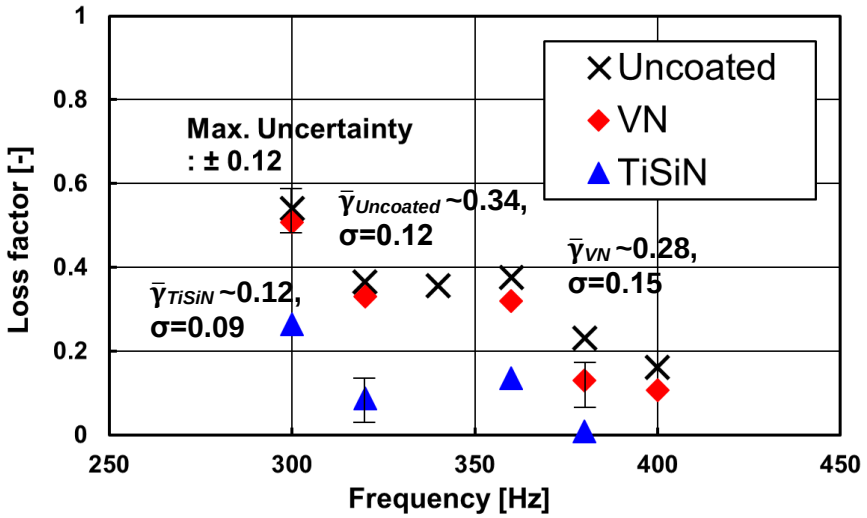

Figure 42. Loss factor (γ) versus excitation frequency for test top foils (one uncoated and three coated). Journal rotation of 50 krpm (833 Hz) with static load of 16 kPa. Average 10 excitations.

The loss factor of prior measurements in Ref. [29] also decreases with an increase in excitation frequency, as shown in Figure 43. γ ceases to decrease for ω > 400 Hz, thus showing a slightly larger magnitude than the current ones. Both current and prior measurements for an uncoated test bearing show a loss factor γ of 0.3~0.5 over the excitation frequency range of 300~400 Hz.

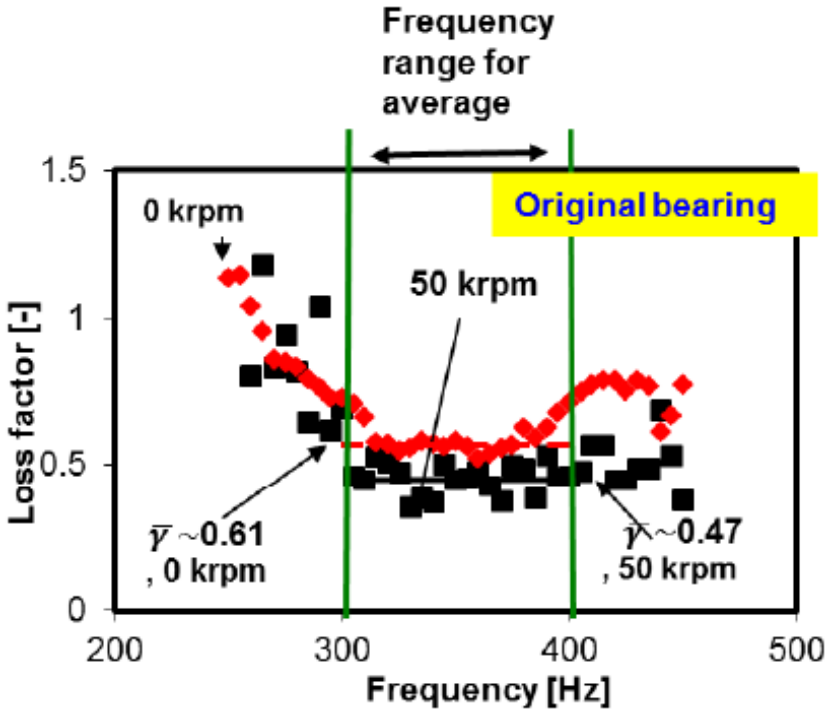

Figure 43. Loss factor (γ) versus excitation frequency for test bearings taken from Ref. [29]. No journal rotation and journal rotation of 50 krpm (833 Hz). Operation with static load of 16 kPa.

Table 7 lists average loss factor[8] ($\bar{\gamma}$) and its standard deviation[9] (σ) over the excitation frequency 300~400 Hz. A too large γ (> 1) is removed due to the smallness of the stiffness coefficients, and the unexpected contacts inside the test bearing which come from the imperfection of rolling test top foils. The table includes the dry-sliding friction coefficient (f_o) taken from Table 6. Figure 44 shows the average loss factor ($\bar{\gamma}$) versus the dry-sliding friction coefficient (f_o) to identify a correlation between them. Recall f_o is obtained from the peak drag torque while the shaft accelerates to a top speed of 70 krpm.

[8] Average loss factor $\bar{\gamma}=\frac{1}{\omega_2-\omega_1}\int_{\omega_1}^{\omega_2}\gamma\, d\omega$, where ω_1 and ω_2 are arbitrary frequency

[9] Standard deviation $\sigma=\sqrt{\frac{\Sigma(\gamma-\bar{\gamma})^2}{n}}$, where n is the number of averaged samples.

Table 7. Correlation between average loss factor ($\bar{\gamma}$) and dry-sliding friction coefficient (f_o) taken from Table 6. σ: Standard deviation.

	$\bar{\gamma}$ (Ω=50 krpm , *W/(LD)*=16 kPa)	$\bar{\gamma}$ (Ω=0 krpm , *W/(LD)*=16 kPa)	f_o (Ω= ~10 krpm at peak torque, *W/(LD)*=8 kPa)
Uncoated	0.34, σ=0.12	0.78, σ=0.14	0.57
VN	0.28, σ=0.15	0.74, σ=0.13	0.38
TiSiN	0.12, σ=0.09	0.64, σ=0.12	0.29

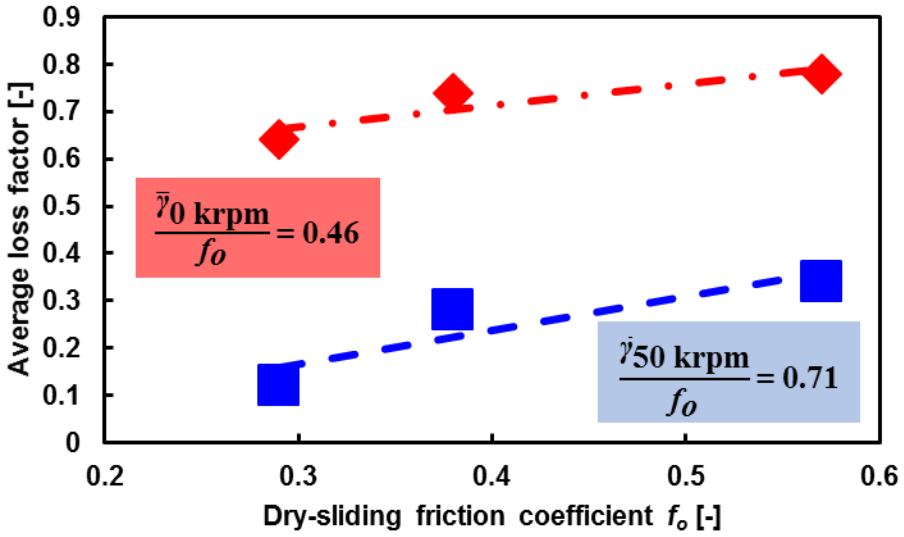

Figure 44. Average loss factor ($\bar{\gamma}$) versus dry-sliding friction coefficient (f_o).

During airborne operation, the distinct dry-sliding friction coefficient (f_o) produced by a coating ($f_{o,Uncoated} > f_{o,VN} > f_{o,TiSiN}$) on the back surface of top foil causes different damping coefficients (Coulomb damping). On the other hand, the bearing stiffness coefficients should be the same for all the test bearings because of their identical geometry and similar under-spring structure.

During the tests, the structural damping and the viscous damping should be the same for all the test bearings since they have same structural characteristics (geometry) and

generate the same gas film viscosity by operating at the same rotational speed of 50 krpm (833 Hz) and load. If all of the test top foils are coated on their front-side only (on surface facing the rotor) and with an uncoated back-side, all the force coefficients of the test bearings should be the same. However, the test top foil with VN or TiSiN is coated on both sides. Hence, the kinetic friction of a metal contact between the top foil and bump strip layers is likely reduced, which generates less Coulomb damping causing less energy dissipations, and thus a lesser loss factor. That is, a decrease in the dry-sliding friction (f_o) decreases the bearing loss factor (γ). Hence, the dry-sliding friction coefficient correlates to the bearing loss factor ($\frac{\bar{\gamma}_{0\ \text{krpm}}}{f_o} = 0.46$, $\frac{\bar{\gamma}_{50\ \text{krpm}}}{f_o} = 0.71$).

Post-test inspection of the test top foils

Figure 45 shows the back side of the test top foils in post-test inspection. In the photograph, wear marks are engraved along surfaces of contacts between the top foil and the bumps, thus evidencing the Coulomb friction causing the Coulomb damping. The wear marks on the test foils with uncoated and coated with VN are more distinct than those on the test foil coated with TiSiN, thus indicating the Coulomb dampings of the uncoated and coated with VN test foils are larger than those of the coated with TiSiN test foil. Consequently, this can explain why the test bearings show different damping coefficients and different loss factors subsequently. Note that the wear marks are rare on the test foil

coated with TiSiN, thus evidencing small magnitude of the damping coefficients (see Figure 41) which can lead the loss factor to be null in the end (see Figure 42).

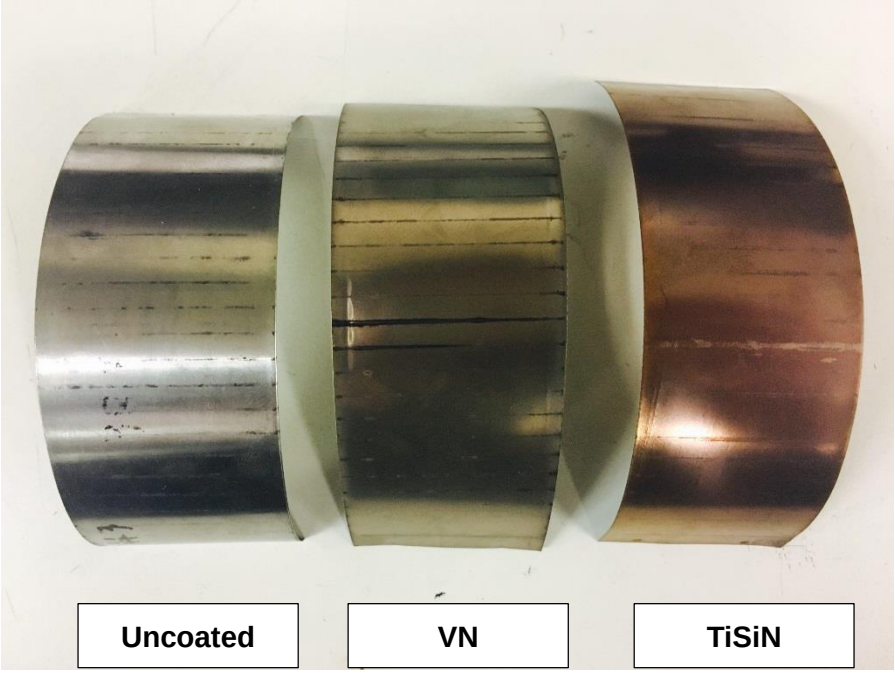

Figure 45. Wear marks on the back side of the test top foils evidencing the Coulomb damping. Post-test inspection.

CHAPTER VI

CONCLUSIONS

This thesis presents measurements characterizing the static and dynamic performance of bump-type foil bearings with their top foils coated with VN, TiSiN (front & back surfaces are coated), and MoS_2 (front surface is coated only), and with a bare top foil (uncoated). Measurements include the dry-sliding friction torque, journal lift-off shaft speed and torque, touch down shaft speed and torque, and the airborne torque. From these measurements, a friction coefficient under dry-sliding and also full hydrodynamic regime is evaluated for operation under various static loads (max. $W/(LD)$=25.4 kPa).

Measurements of rotordynamic force coefficients for the test bearings are conducted without shaft rotation and with rotation of 50 krpm and with dynamic loads over a range of excitation frequency (200-400Hz). All measurements took place at a facility operating at room temperature (~20ºC).

Dry-sliding friction torque measurements

1) The dry-sliding friction torque of the uncoated (top) foil bearing is lower than those for the bearings having coated top foils. The bearing with a top foil coated with a VN layer shows the largest dry-sliding friction torque.
2) The estimated dry-sliding friction factor (f_o) decreases as the specific load ($W/(LD)$) increases.

3) Journal rotation towards the top foil free end determines a bearng has a larger f_o than for rotations in reverse.

Drag torque measurements during rotor acceleration and deceleration tests

1) In general, the bearings with a coated top foil have a lesser drag torque than that with the uncoated top foil bearing. Among the coated foil bearings, the bearing with VN coating shows the highest drag torque, whereas the one with MoS_2 shows the lowest drag torque.
2) The drag torque increases with an increase in applied static load.
3) The averaged lift-off speed of the bearing with uncoated top foil is higher than ~30 krpm while that of the bearing with MoS_2 coating is lower than ~20 krpm and those of the bearing with either VN coating or TiSiN coating are in between 20~30 krpm.
4) The average touch down speeds of the bearings seem to be on 20~30 krpm, except the one with TiSiN coating over 40 krpm. Generally, the airborne torque is too small (less than ~10% of peak torque).
5) When the rotor starts up, the dry-sliding friction coefficient f_o of the bearing with VN coating is ~0.4 while f_o for the bearing with TiSiN coating is 0.3~0.4. The uncoated bearing has the highest dry-sliding friction coefficient f_o of ~0.6, and the MoS_2 coated one has the lowest f_o of 0.2~0.3.

Rotordynamic force coefficients tests

1) The direct stiffness coefficients ($\underline{K_{XX}}$=$\underline{K_{YY}}$) increase with excitation frequency, being larger for the 16 kPa condition than without an applied load.
2) The BFB $\underline{K_{XX}}$=$\underline{K_{YY}}$ with journal rotation of 50 krpm (833 Hz) are smaller than those without journal rotation, which means the presence of a gas film acting in series with the under-spring structure hence reduces the BFB stiffnesses.
3) The damping coefficients are inversely proportional to frequency, i.e., diminishing with frequency. The direct damping coefficients ($\underline{C_{XX}}$=$\underline{C_{YY}}$) are larger under an applied specific load of 16 kPa than those without a static load.
4) The BFB $\underline{C_{XX}}$=$\underline{C_{YY}}$ with journal rotation of 50 krpm (833 Hz) have lower magnitude than those coefficients without journal rotation. This is because the gas film acts in a series with its under-spring structure.
5) The stiffness coefficients are largely determined by the under spring structure, while the BFB damping coefficient are largely affected by a dry-sliding friction coefficient (Coulomb friction) of coating on back surface of the top foil.
6) The bearing loss factor decreases with increasing excitation frequency. The variation in the loss factor with frequency is due to the force coefficients which also vary with frequency.
7) The bearing loss factor of the coated with VN test bearing shows comparable magnitude ($\bar{\gamma}$~0.28) with that of the uncoated one ($\bar{\gamma}$~0.34), while indicating

that the VN coated bearing dissipates more energy during full film operation than the coated with TiSiN test bearing ($\bar{\gamma}$~0.12).

In conclusion, the VN and TiSiN coated top foils (front & back surfaces) reduce the energy loss (less dry-sliding friction than the uncoated top foil) of a test bearing during rotor start up and shut down events. That is, the kinetic friction of a metal contact between the top foil and bump strip layers is likely reduced, which generates less Coulomb damping causing less energy dissipations, and thus a lesser loss factor. Hence, coating the back surface of top foil reduces the loss factor; at a high frequency (> 350 Hz), in particular. The test data show the bearing dry-sliding friction coefficient has a strong correlation with the bearing loss factor ($\frac{\bar{\gamma}_{0\ \mathrm{krpm}}}{f_o} = 0.46$, $\frac{\bar{\gamma}_{50\ \mathrm{krpm}}}{f_o} = 0.71$).

The coating on a top foil can be implemented for a high temperature applications only if it works at room temperature first. In this thesis, tests on top foil coating conducted at room temperature evidence less f_o for a coated top foil bearing than the f_o for an uncoated top foil. Therefore, the tested BFBs with a top foil coating can be applied to high temperature endurance experiments.

REFERENCES

[1] Agrawal, G.L., 1997, “Foil Air/Gas Bearing Technology – an Overview”, ASME Paper No. 97-GT-347.

[2] Kim, T.H., and San Andrés, L. 2008, “Forced Nonlinear Response of Gas Foil Bearing Supported Rotors”, Tribol. Int., **41**, pp. 704-715.

[3] San Andrés, L., Rubio, D., and Kim, T.H., 2007, “Rotordynamic Performance of a Rotor Supported on Bump Type Foil Gas Bearings: Experiments and Predictions”, ASME J. Eng. Gas Turbines Power, **129(3)**, pp. 850-857.

[4] Chen, H.M., Howarth, R., Geren, B., Theilacker, J.C., and Soyars, W.M., 2001, “Application of Foil Bearings to Helium Turbocompressors”, Proceedings Of 30th Turbomachinery Symposium, Houston, TX., September 22-25, 2001.

[5] DellaCorte. C., Radil, K.C., Bruckner, R.J., and Howard, S.A., 2008, “Design, Fabrication, and Performance of Open Source Generation I and II Compliant Hydrodynamic Gas Foil Bearings”, STLE Tribol. Trans., **51**, pp. 254-264.

[6] Blok, H., and van Rossum, J.J., 1953, “The Foil Bearing – A New Departure in Hydrodynamic Lubrication”, Lubr. Eng., December, pp. 316-320.

[7] Kim, T.H., and San Andrés, L., 2009, “Effects of a Mechanical Preload on the Dynamic Force Response of Gas Foil Bearings - Measurements and Model Predictions”, STLE Tribol. Trans., **52**, pp. 569-580.

[8] Lee, Y.B., Suk, B.K., Kim, T.H., and Sim, K., 2013, “Feasibility of an Oil-Free Turbocharger Supported on Gas Foil Bearings via On-Road Tests of a Two-Liter Class Diesel Vehicle”, ASME J. Eng. Gas Turbines Power, **135**, p.052701-1.

[9] Kicinski, J., Zywica, G., and Baginski, P., 2014, “Thermal Studies on Foil Bearings With a Sliding Coating Made of Plastic Material”, 9th IFToMM International Conference on Rotor Dynamics, pp. 1183–1193.

[10] DellaCorte, C., Zaldana, A.R. and Radil, K.C., 2004, “A Systems Approach to the Solid Lubrication of Foil Air Bearings for Oil-Free Turbomachinery”, J. Tribol **126(1)**, pp.200-207.

[11] Heshmat, H., Hryniewicz, P., Walton. J, 2005, “Low-Friction Wear-Resistant Coatings for High-Temperature Foil Bearings”, Tribol. Int., **41**, pp. 1059-1075

[12] Jahanmir, S., Heshmat, H. and Heshmat, C., 2009, “Assessment of Tribological Coatings for Foil Bearing Applications”, STLE Tribol. Trans., **52(2)**, pp. 231-242.

[13] Kim, D., and Zimbru, G., 2012, “Start-Stop Characteristics and Thermal Behavior of a Large Hybrid Airfoil Bearing for Aero-Propulsion Applications”, ASME J. Eng. Gas Turbines Power, **134(3)**, p.032502.

[14] Aouadi, S.M., Gao, H., and Martini, A., 2014, “Lubricious Oxide Coatings for Extreme Temperature Applications: A review”, Surface and Coatings Tech., **257**, pp 266-277

[15] DellaCorte, C., and Edmonds, B.J., 2014, “High Temperature Solid Lubricant Coating for High Temperature Wear Applications”, US 8753417 B1.

[16] Zywica, G., Baginski, P, and Banaszek, S., 2016, “Experimental Studies on Foil Bearing with a Sliding Coating Made of Synthetic Material”, J. Tribol **138(1)**, 011301.

[17] Radil, K., and DellaCorte, C., 2016, “The Performance of PS400® Subjected to Sliding Contact at Temperatures from 260 to 927 ºC”, STLE Tribol. Trans., DOI: 10. 1080/10402004.2016. 1231357

[18] Sim, K. and Park, J., 2017, “Performance Measurements of Gas Bearings With High Damping Structures of Polymer and Bump Foil Via Electric Motor Driving Tests and One Degree-of-Freedom Shaker Dynamic Loading Tests”, ASME J. Eng. Gas Turbines Power, **139(9)**, p.092504.

[19] Chirathadam, T. A., and San Andrés, L., 2012, “A Metal Mesh Foil Bearing and a Bump- Type Foil Bearing: Comparison of Performance for Two Similar Size Gas Bearings”, ASME J. Eng. Gas Turbines Power, **134**, p.102501.

[20] Ryu, K., and San Andrés, L., 2013, “On the Filure of a Gas Foil Bearing: High Temperature Operation Without Cooling Flow”, ASME J. Eng. Gas Turbines Power, **135**, p.112506

[21] San Andrés, L., and Norsworthy, J., 2016, “Structural and Rotordynamic Force Coefficients of a Shimmed Bump Foil Bearing: An Assessment of a Simple Engineering Practice”, ASME J. Eng. Gas Turbines Power, **138**, p.012505

[22] Ryu, K., and Ashton, Z., 2017, “Oil-Free Automotive Turbochargers: Drag Friction and On-Engine Performance Comparisons to Oil-Lubricated Commercial Turbochargers”, ASME J. Eng. Gas Turbines Power, **139**, p.032301

[23] San Andrés, L., and Norsworthy, J., 2013, “Identification of Structural Stiffness and Material Loss Factor in a Shimmed (Generation One) Bump-Type Foil Bearing”, TRC-B&C-04-13, Annual Progress Report to the Turbomachinery Research Consortium, May. Mechanical Engineering, Texas A&M University, College Station, TX.

[24] Lee, Y.B., Kwon, S.B., Kim, T.H., and Sim, K.H., 2013, “Feasibility Study of an Oil-Free Turbocharger Supported on Gas Foil Bearings Via On-Road Tests of a Two-Liter Class Diesel Vehicle”, ASME J. Eng. Gas Turbines Power, **135(5)**, p.052701.

[25] Feng, K., Zhao, X., and Guo, Z., 2015, “Design and Structural Performance Measurements of a Novel Multi-Cantilever Foil Bearing”, J. Mechanical Engineering Science, **229(10)**, pp. 1830-1838.

[26] Feng, K., and Zhao, X., 2015, “Effects of Misalignment on the Structure Characteristics of Bump-Type Foil Bearings”, Industrial Lubrication and Tribology, **67(4)**, pp. 370-379.

[27] Rubio, D., and San Andrés, L., 2006, “Bump-Type Foil Bearing Structural Stiffness: Experiments and Predictions”, ASME J. Eng. Gas Turbines Power, **128**, pp. 653-660.

[28] Chirathadam, T.A., 2012, “Metal Mesh Foil Bearings: Prediction and Measurement of Static and Dynamic Performance Characteristics”, Ph.D Dissertation, Texas A&M University, College Station, TX.

[29] Norsworthy, J., 2014, “Measurement of Drag Torque, Lift Off Speed, and Identification of Frequency Dependent Stiffness and Damping Coefficients of a Shimmed Bump-Type Foil Bearing”, Master Thesis, Texas A&M University, College Station, TX.

APPENDIX A

UNCERTAINTY AND VARIABILITY OF TEST RESULTS

This section outlines the calculation of uncertainty and discussion of variability in the drag torque measurements and the experimentally identified BFB force coefficients. The instrument uncertainty of the accelerometers, load cells, and eddy current sensors is 1% linearity.

A.1 Uncertainty in the drag torque measurements

The uncertainty in drag torque ($T=\delta K_s L_T$) measurements is due to the uncertainty in the measurement of position (δ), the spring stiffness (K_s), and the measurement of the torque arm (L_T). The torque arm is measured with calipers, uncertainty~ ±.0001mm (U_L). The uncertainty in the position measurement is ±0.70 μm (U_x). The spring stiffness is estimated from load deflection tests. The spring stiffness is identified as the slope of the load deflection curve, which is linear. The uncertainty in the spring stiffness is (±0.33 N/mm). The Cline-McClintock method of evaluating measurement uncertainty delivers a general uncertainty formulation for a function of multiple variables ($r=f(x_1, x_2,\ldots\ldots,x_n)$). The general equation for the uncertainty of a function with multiple variables is

$$U_r=\sqrt{\left(\frac{\partial r}{\partial x_1}U_{x_1}\right)^2+\left(\frac{\partial r}{\partial x_2}U_{x_2}\right)^2+\cdots+\left(\frac{\partial r}{\partial x_n}U_{x_n}\right)^2} \qquad \text{(A.1)}$$

Using the above equation, the uncertainty of the drag torque (U_T) is identified from the following equation.

$$\left(\frac{U_T}{T}\right)^2 = \left(\frac{U_x}{x}\right)^2 + \left(\frac{U_K}{K}\right)^2 + \left(\frac{U_{L_T}}{L_T}\right)^2 \quad \text{(A.2)}$$

From this equation, the uncertainty in the measured drag torque is ± 1 N-mm.

A.2 Variability in the drag torque measurements

Drag torque measurements are conducted for uncoated and coated (TiSiN, VN, MoS_2) bearings. The bearing drag torque is recorded for rotor speeds up to 70 krpm. Figure A.1 shows the drag torque results and their variability for three tests for uncoated and coated bearing. The variability of the drag torque measurements prior to lift off (< 20 krpm) is difficult to access, however the variability of the drag torque measurements after lift-off is identified. The maximum variability occurs for test conducted on the uncoated bearing, ~15 N-mm. The drag torque results agree very well between individual tests and show very little variance.

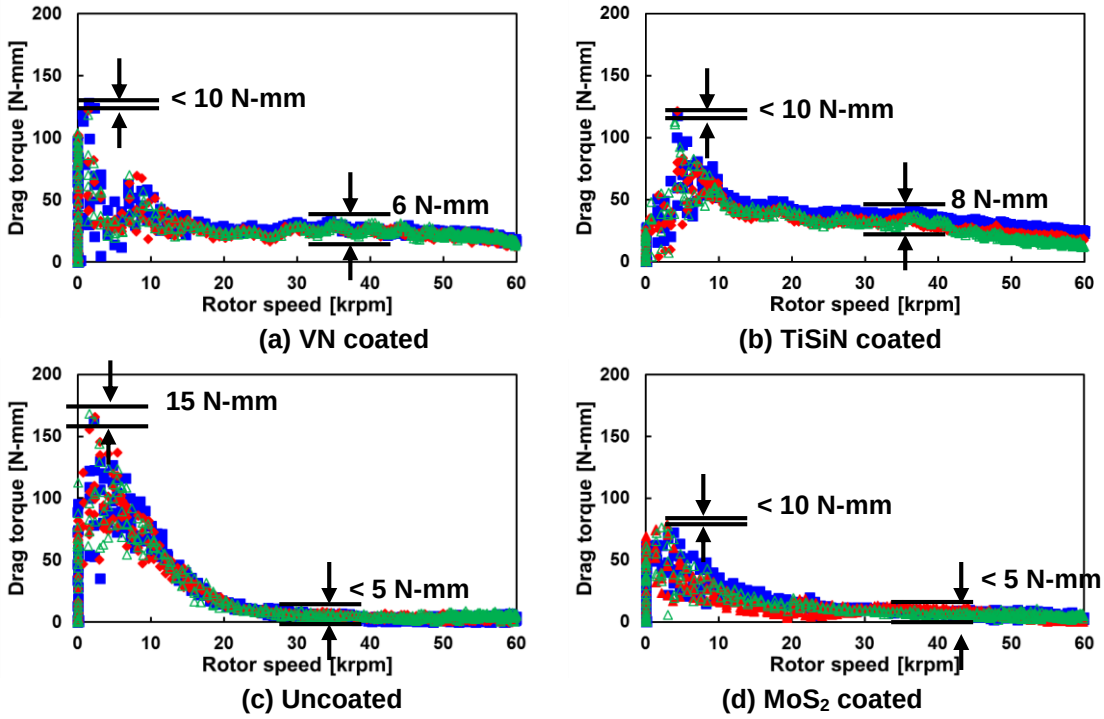

Figure A1. Bearing drag torque versus rotor speed for uncoated and coated test bearings. Applied static load of 16 kPa. Results for three tests are shown.

A.3 Uncertainty in the force coefficients

Uncertainty in the bearing force coefficients arises from the instrumentation uncertainty in the measurements of bearing cartridge accelerating, bearing relative displacement and excitation force. Assuming the uncertainties of both directions (X, Y) are approximately equal, the uncertainty in the bearing impedance is computed by using equation A.1.

$$\left(\frac{U_{H_{xx}}}{H_{xx}}\right) = \frac{1}{\sqrt{2}}\sqrt{\left(\frac{U_{G_{xx}}}{G_{xx}}\right)^2 + \left(\frac{U_{X_x}}{X_x}\right)^2} \tag{A.3}$$

The fractional uncertainties in the dynamic load $\left(\frac{U_F}{F}\right)$, acceleration $\left(\frac{U_A}{A}\right)$ and the excitation frequency $\left(\frac{U_\omega}{\omega}\right)$ are less than 0.02, 0.01, and 0.05 respectively. The resulting

maximum uncertainty in the stiffness and damping coefficients is ±0.08 MN/m and ±80 Ns/m, respectively.

A.4 Variability in the force coefficients

A minimum of three tests are conducted for each load condition to asses and verify the repeatability of the identification process. Figures A.2 and A.3 show the bearing stiffness and damping coefficients from three independent tests. The repeated tests are conducted on the VN coated test bearing.

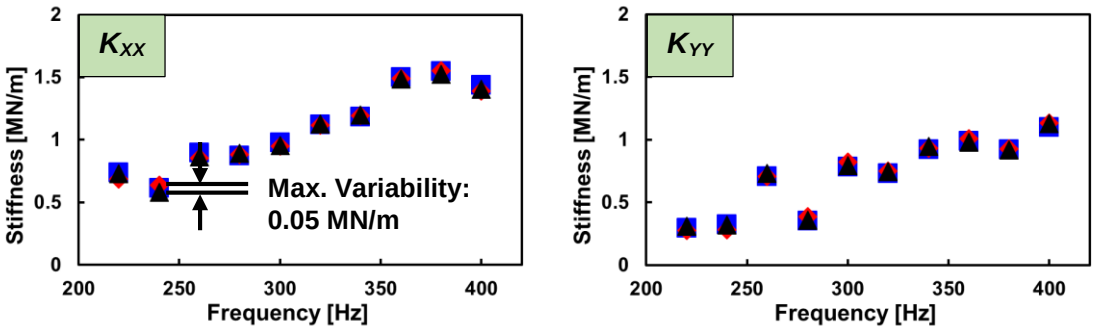

Figure A2. Identified BFB stiffness coefficients versus frequency. Static load of 16.0 kPa. Journal rotation at 50 krpm (833 Hz). Results for three tests shown.

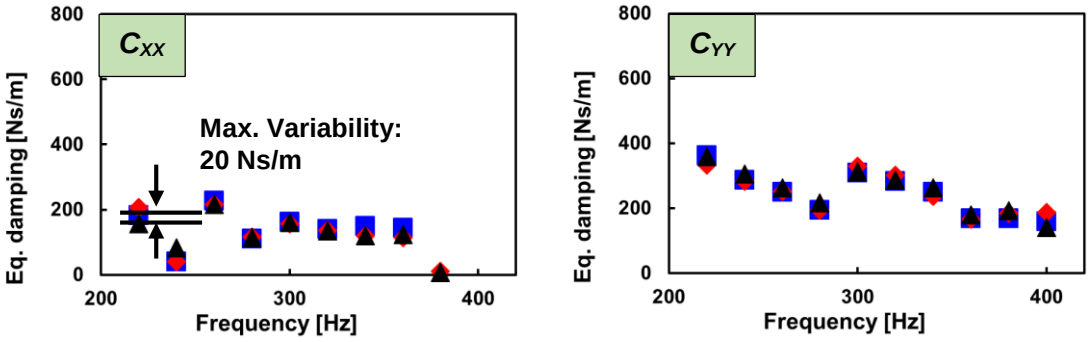

Figure A3. Identified BFB damping coefficients versus frequency. Static load of 16.0 kPa. Journal rotation at 50 krpm (833 Hz). Results for three tests shown.

The maximum variability in the K_{XX} is less than 0.05 MN/m while the K_{YY} is almost null for whole frequency range. Also, the maximum variability for C_{XX} and C_{YY} are less than 20 Ns/m, repectively. The test data indicates that the tests are reliable and repeatable.

APPENDIX B

IMPACT LOAD TESTS TO IDENTIFY STRUCTURE FORCE COEFFICIENTS

A soft elastic structure, squirrel cage comprise of 8 thin steel rods arranged in a circular pattern. Before the tests, the radial stiffness and damping coefficients of squirrel cage have to be determined first. The excitations are applied orthogonal to each other along the *X* and *Y* directions.

Since there is little structural cross coupling, the bearing and squirrel cage behave as a single degree of freedom system along each direction. The system is characterized by a system mass (M_S), stiffness (K_S), and viscous damping (C_S) coefficients along each direction (*X*,*Y*). The measurements of acceleration and impact load are used to extract the structural parameters according to a nonlinear curve fit of the accelerance function. The accelerance function along the *X* direction is

$$\left|\frac{a_{X(\omega)}}{F_{X(\omega)}}\right| = \frac{\omega^2}{\sqrt{\left\{\left(K_{S_X}-\omega^2 M_{S_X}\right)^2+\left(\omega C_{S_X}\right)^2\right\}}} \qquad \text{(B.1)}$$

where ω denotes frequency. Figure B1 shows the recorded accelerance function $\left|\frac{a_{X(\omega)}}{F_{X(\omega)}}\right|$ and its curve fit equation. The identified mass is M_{S_X}=1.2 kg including the mass of the bearing (1.0 kg, measured on a scale), and the squirrel cage structure displaced during excitation. The identified structural stiffness K_{S_X}=17 kN/m, and the damping coefficient C_{S_X}=6.4 Ns/m. The goodness to fit is R^2=0.95 for the frequency range.

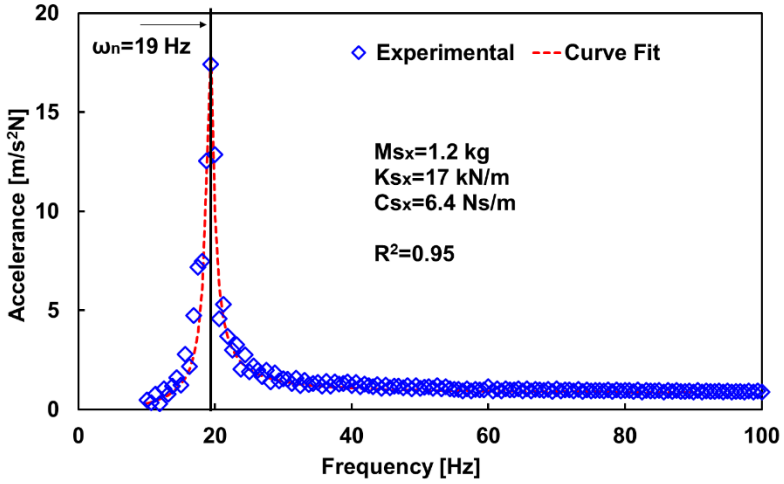

Figure B1. Accelerance $|a_X/F_X|$ and curve fit to identify parameters of bearing elastic support structure.

Likewise, figure B2 shows the recorded accelerance function $\left|\frac{a_{Y(\omega)}}{F_{Y(\omega)}}\right|$ and its curve fit equation. The identified parameters include the identified mass M_{S_Y}=1.3 kg, the identified structural stiffness K_{S_Y}=16 kN/m, and damping coefficient C_{S_Y}=6.6 Ns/m, and the goodness to fit is R^2=0.94 for the frequency range.

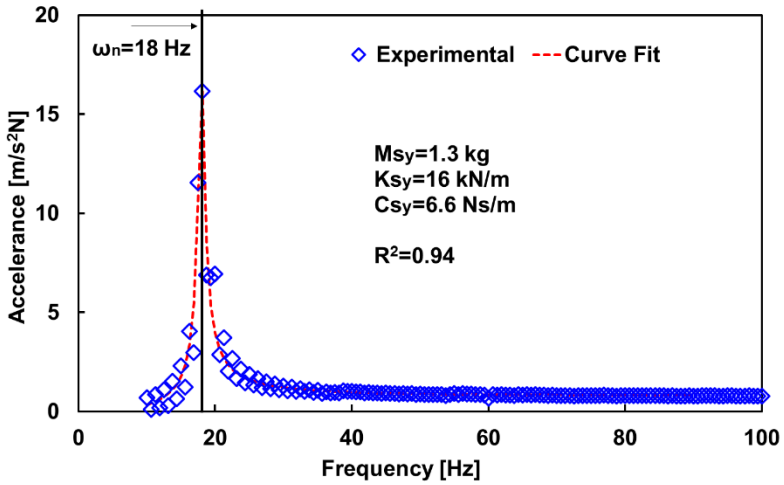

Figure B2. Accelerance $|a_Y/F_Y|$ and curve fit to identify parameters of bearing elastic support structure.

Table B1 lists the identified bearing structural coefficients along *X* and *Y* directions, which shows the system is not isotropic even though they are quite similar.

Table B1. Measured mechanical parameters for bearing and elastic support structure (from 3 independent tests).

Parameters	Directions		Unit
	X	Y	
Mass, M_S	1.2±0.01	1.3±0.22	kg
Stiffness, K_S	17.4±0.2	16.9±2.9	kN/m
Damping, C_S	6.0±3.3	5.4±2.5	N.s/m
Damping ratio	0.02	0.02	-
Natural frequency	19±0.5	18±0.5	Hz
R^2	0.95	0.94	-